Graphical Abstract (for review)

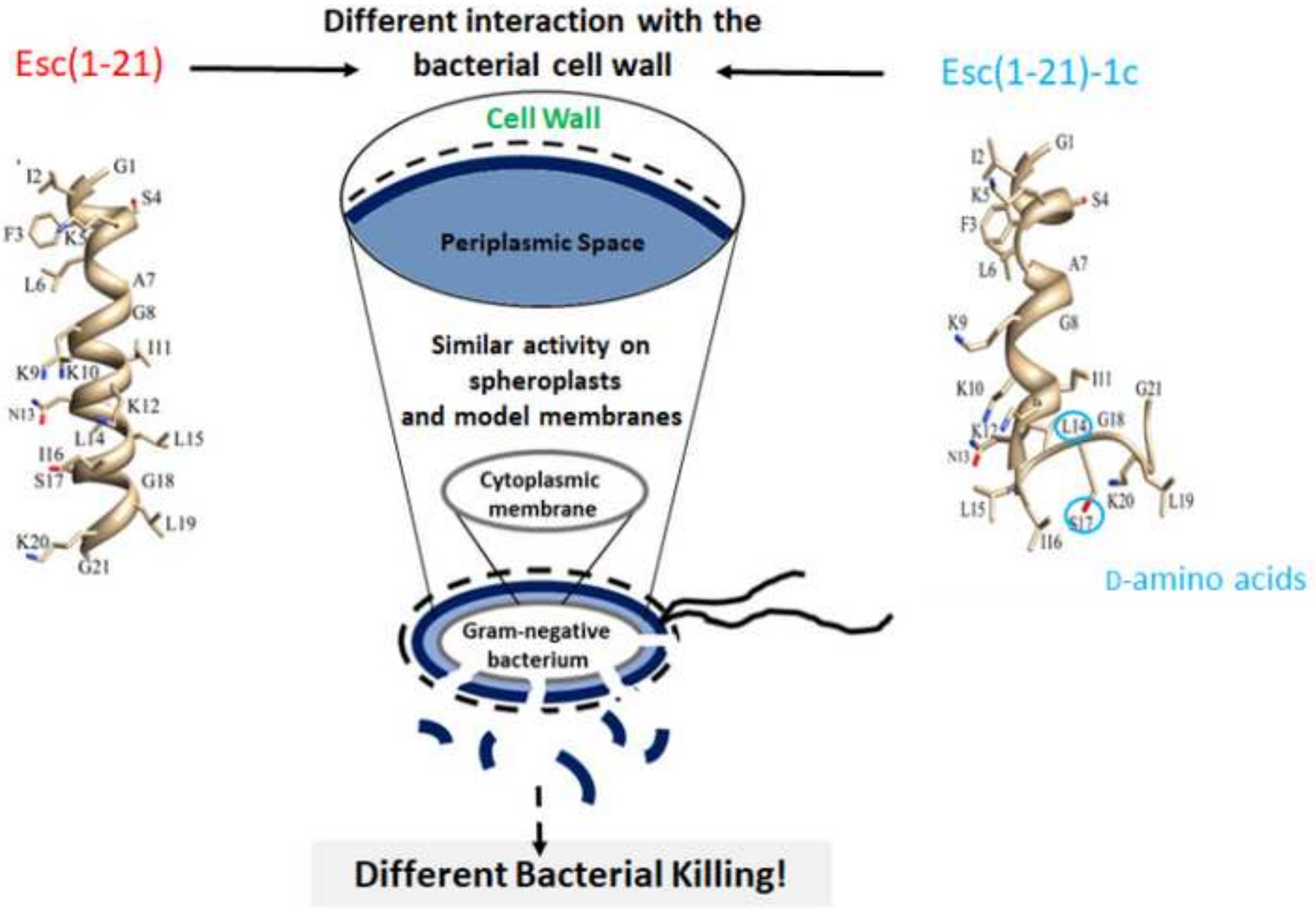

Highlights

-The presence of ^{D}Leu14 and ^{D}Ser17 in Esc(1-21) reduces α-helix and cytotoxicity

-Both isomers have similar effects on model membranes and spheroplasts

-The different activity involves interaction with the bacterial cell wall

Membrane Perturbing Activities and Structural Properties of the Frog-skin Derived Peptide Esculentin-1a(1-21)NH_2 and its Diastereomer Esc(1-21)-1c: Correlation With Their Antipseudomonal and Cytotoxic Activity

Maria Rosa Loffredo[*,1] Anirban Ghosh[*,2] Nicole Harmouche,[3] Bruno Casciaro[1], Vincenzo Luca[1], Annalisa Bortolotti[4], Floriana Cappiello[1], Lorenzo Stella[4], Anirban Bhunia[2], Burkhard Bechinger,[3] and Maria Luisa Mangoni[1#]

*The authors equally contributed to the work

[1] Laboratory affiliated to Pasteur Italia-Fondazione Cenci Bolognetti, Department of Biochemical Sciences, Sapienza University of Rome, Rome, via degli Apuli, 9-00185, Italy; [2]Department of Biophysics, Bose Institute, P-1/12, CIT Road, Scheme VII (M), Kolkata 700054, India; [3]University of Strasbourg/CNRS, Chemistry Institute UMR 7177, 4 rue Blaise Pascal, 67070 Strasbourg, France; [4]University of Rome Tor Vergata, Department of Chemical Sciences and Technologies, 00133 Rome, Italy

To whom correspondence should be addressed

Maria Luisa Mangoni, PhD
Department of Biochemical Sciences,
Sapienza University of Rome.
Via degli Apuli, 9-00185, Rome-Italy;
Phone: +39 06 49917693
Fax: +39 0649917566
Email: marialuisa.mangoni@uniroma1.it

Abstract

Antimicrobial peptides (AMPs) represent new alternatives to cope with the increasing number of multi-drug resistant microbial infections. Recently, a derivative of the frog-skin AMP esculentin-1a, Esc(1-21), was found to rapidly kill both the planktonic and biofilm forms of the Gram-negative bacterium *Pseudomonas aeruginosa* with a membrane-perturbing activity as a plausible mode of action. Lately, its diastereomer Esc(1-21)-1c containing two D-amino acids i.e. ^{D}Leu14 and ^{D}Ser17 revealed to be less cytotoxic, more stable to proteolytic degradation and more efficient in eradicating Pseudomonas biofilm. When tested *in vitro* against the free-living form of this pathogen, it displayed potent bactericidal activity, but this was weaker than that of the all-L peptide. To investigate the reason accounting for this difference, mechanistic studies were performed on Pseudomonas spheroplasts and anionic or zwitterionic membranes, mimicking the composition of microbial and mammalian membranes, respectively. Furthermore, structural studies by means of optical and nuclear magnetic resonance spectroscopies were carried out. Our results suggest that the different extent in the bactericidal activity between the two isomers is principally due to differences in their interaction with the bacterial cell wall components. Indeed, the lower ability in binding and perturbing anionic phospholipid bilayers for Esc(1-21)-1c contributes only in a small part to this difference, while the final effect of membrane thinning once the peptide is inserted into the membrane is identical to that provoked by Esc(1-21). In addition, the presence of two D-amino acids is sufficient to reduce the α-helical content of the peptide, in parallel with its lower cytotoxicity.

Keywords: antimicrobial peptides; esculentin; liposomes; *Pseudomonas aeruginosa*; spheroplasts; membrane thinning

1. Introduction

Most living organisms produce gene-encoded antimicrobial peptides (AMPs) as readily available weapons against a wide variety of microbial pathogens [1-3]. The majority of these AMPs are cationic molecules at neutral pH and they adopt an amphipathic α-helical structure in membrane environments [4]. These two remarkable features are fundamental for their broad microbicidal activity, which generally relies on the perturbation of the target cell membrane, thus limiting the induction of resistance [1, 5]. Their ability to recognize and distinguish bacterial membranes from those of mammalian cells is based on an initial electrostatic interaction between the positively charged residues of the peptide and the negatively charged membrane phospholipids [6, 7]. The latter are much more abundant at the outside of microbial cells when compared to the external leaflet of mammalian cell membranes, which are mostly made of zwitterionic phosphatidylcholine and sphingomyelin [5]. However, in the case of Gram-negative bacteria, before reaching the cytoplasmic membrane (i.e. inner membrane), bacteria need to cross the lipopolysaccharide (LPS)-outer layer in a self-promoted uptake mechanism [8]. Subsequently, the phospholipid bilayer of the inner membrane is destabilized via pore formation or micellization, leading to cell death [9-11]. After membrane passage, inner targets may also exist for some of the peptides [12, 13]. In contrast, conventional antibiotics generally inhibit intracellular biological function(s) upon interaction with a single stereospecific target that can be mutated [14, 15], making it easier for the microbes to become resistant to this class of drugs [16, 17]. Due to the alarming worldwide emergence of multi-drug resistant (MDR) pathogenic microorganisms [18] and the concomitant decrease in the pharmaceutical industry research pipeline for novel antibiotics, the search for new antimicrobial strategies has become strictly necessary [19-21]. AMPs hold promise for the development of new anti-infective compounds [22-25]. Interestingly, a few years ago we discovered that a short-sized AMP, esculentin-1a(1-21)NH_2, Esc(1-21), derived from a natural AMP of amphibian origin was

endowed with: (i) wide and potent spectrum of activity especially against Gram-negative bacteria [26-28] and (ii) rapid killing kinetics on planktonic and biofilm cells of *Pseudomonas aeruginosa*. It also showed a membrane-perturbing activity as a plausible mode of action [29]. In addition, it was found to have additional non-antimicrobial properties. Among those, the ability (i) to detoxify *P. aeruginosa* LPS [30] and (ii) to induce re-epithelialization of a pseudo-"wound"; a property which is not shown by any traditional antibiotic [30, 31].

Furthermore, we recently demonstrated that a diastereomer of Esc(1-21), named Esc(1-21)-1c, containing two D-amino acids i.e. ^{D}Leu14 and ^{D}Ser17 had significant lower cytotoxicity and higher biostability than its all-L isomer [30]. Yet, it was more efficient in promoting clearance of *P. aeruginosa* internalized in bronchial cells as well as in stimulating wound-healing in an *in vitro* bronchial epithelial cells model [32]. However, when tested *in vitro* against the free living form of *P. aeruginosa* strains, even if it displayed a potent killing activity this was weaker than the parent Esc(1-21) [32].

With the aim to understand whether this discrepancy reflected a different ability of the peptides in damaging the cytoplasmic membrane of bacterial cells or a different interaction with the bacterial cell surface, mechanistic studies have been performed on intact bacterial cells, with bacteria devoid of their cell wall (i.e. spheroplasts) as well as micelles mimicking the head group composition and/or surface charge of membranes. In parallel, to verify whether the lower cytotoxicity of the diastereomer in comparison to the all-L peptide reflected a weaker ability in destabilizing zwitterionic membranes, the leakage of a fluorescent marker from neutral lipid vesicles was assessed in comparison to anionic vesicles. Furthermore, by using optical and nuclear magnetic resonance spectroscopies, the secondary structure of the peptides in membrane-mimicking environments has been investigated. Our studies revealed that the weaker *in vitro* antimicrobial activity of the two D-amino acid containing Esc(1-21)-1c in comparison with the all-L Esc(1-21) is mainly associated to a different interaction of the peptide with microbial cell wall components and

only partially due to a weaker ability in binding and perturbing anionic membranes. Furthermore, the presence of two D-amino acids was found to be sufficient to reduce the α-helical content of the peptide, in line with its lower cytotoxicity.

2. Materials and Methods

2.1. Materials

Synthetic Esc(1-21) and its diastereomer Esc(1-21)-1c (Scheme 1) were purchased from Chematek Spa (Milan, Italy). Each peptide was assembled by stepwise solid-phase synthesis using a standard F-moc strategy and purified via reverse-phase high-performance liquid chromatography (RP-HPLC) to a purity of 98%, while the molecular mass was verified by mass spectrometry. The following lipids: 1-palmitoyl-2-oleoyl-*sn*-glycero-3-phosphoethanolamine (POPE); 1-palmitoyl-2-oleoyl-*sn*-glycero-3-phosphoglycerol (POPG); 1-palmitoyl-2-oleoyl-*sn*-glycero-3-phosphocholine (POPC), POPE-$^{2}H_{31}$ and cholesterol (Cho) were purchased from Avanti Polar Lipids (Alabaster, AL, USA). Sodium-dodecylsulfate (SDS), dodecylphosphocholine (DPC) were obtained from Cambridge Isotope Laboratory (Tewksbury, MA); carboxyfluorescein (CF), water (HPLC grade), deuterium depleted water, 3-(4,5-dimethylthiazol-2-yl)-2,5-diphenyltetrazolium bromide (MTT) were from Sigma (St. Quentin Fallavier, France). Sytox Green was from Molecular Probes (Invitrogen, Carlsbad, CA, USA).

2.2. Microorganisms

The following bacterial strains were used for the antimicrobial assays: the standard *P. aeruginosa* PAO1 [29] and the clinical isolate *P. aeruginosa* AA43 from the strains collection of the cystic fibrosis clinic Medizinische Hochschule of Hannover, Germany [33].

2.3. Spheroplasts preparation

Spheroplasts of *P. aeruginosa* PAO1 were prepared by adapting the procedure described in [34]. Briefly, bacteria from a log-phase culture were collected by centrifugation at 3,000 x *g* and washed in 0.01 M phosphate buffer, pH 7.0 (PB). The cells were then harvested by centrifugation and resuspended in half-volume of 0.5 M sucrose solution in PB to induce plasmolysis. Lysozyme was added to the cell suspension at a final concentration of 50 μg/ml. After incubation at 37 °C for 90 min with moderate shaking, the sample was diluted 1:1 with PB and ethylenediaminetetraacetic acid (EDTA) was added to a final concentration of 10 mM. The cell suspension was incubated again at 37 °C for additional 60 min. Thereafter, transition of the rod-shaped bacteria into spheres was determined by light microscopy. When ~80% of the cells were spheroplasted (as visualized by phase-contrast microscopy), the reaction was stopped by pelleting the cells at 500 x *g* for 15 min. The spheroplasts were then washed in 0.25 mM sucrose in PB (SPB2), centrifuged at 500 x *g* for 15 min, and resuspended in SPB2.

2.4. Antimicrobial activity

Aliquots of 100 μl of SPB2 containing spheroplasts derived from $1x10^7$ intact bacteria were treated with Esc(1-21) and its diastereomer for 30 min at 37 °C. Afterwards, spheroplasts viability was assayed by the reduction of MTT to insoluble formazan. Briefly, 100 μl of 1 mg/ml MTT were added to the bacterial suspension, transferred into a 96-wells microplate, which was incubated for 90 min at 37 °C. The reduced formazan was then solubilized by the addition of an equal volume of 10% (w/v) SDS, measured in a microplate reader (Infine M 200, Tecan) at 590 nm. All assays were performed in triplicate, and the experiments were repeated three times.

2.5. Sytox Green assay on intact bacterial cells

The ability of the peptide to alter the membrane permeability of whole *Pseudomonas* cells was assessed by the Sytox Green (~ 660 Da) assay. Approximately $1x10^6$ cells in 100 μl of phosphate

buffered saline (PBS) were mixed with 1 μM Sytox Green for 5 min in the dark. After adding peptides at different concentrations, the increase of fluorescence, due to the binding of the dye to intracellular DNA, was measured at 37 °C in the microplate reader (Infinite M200). The excitation and emission wavelengths were 485 and 535 nm, respectively. Cells not exposed to the peptides were used as control, whereas the maximal membrane perturbation was obtained after treating bacteria with the highest peptide concentration used (32 μM) followed by the addition of 1 mM EDTA + 0. 5 % Triton X-100 (final concentration) to completely destabilize the LPS-outer membrane and to solubilize the cytoplasmic membrane [35]. Samples were run in triplicate and the experiments were performed three times.

2.6. Preparation of large unilamellar vesicles (LUVs)

Lipid films of POPE/POPG and POPC/Cho were prepared by dissolving lipids (2 mg of POPE/POPG mixture, 7:3, mol/ mol or 2 mg of POPC/Cho, 1:1, mol/mol) in chloroform/methanol (2:1, v/v). The solvents were then evaporated under reduced argon atmosphere until a thin film was formed. Complete evaporation was ensured by applying a rotary vacuum pump for at least 2 h. The lipid film was then hydrated with a 10 mM phosphate buffer containing 140 mM NaCl and 0.1 mM EDTA, pH 7.4 (buffer A), or with a CF solution at a self-quenching concentration, i.e. 30 mM (for CF leakage experiments) in 10 mM phosphate buffer containing 80 mM NaCl and 0.1 mM EDTA, brought to pH 7.4 with NaOH. The liposome suspension was subjected to 10 freeze and thaw cycles and extruded for 31 times through two stacked polycarbonate membranes with 100 nm pores to obtain LUVs. The free CF (when present) was removed by gel filtration, using a 40 cm Sephadex G-50 at room temperature, equilibrated with buffer A. NaF was used in place of NaCl for CD experiments, to avoid the high absorption by Cl-ions in the far UV [36]. The final lipid concentration was determined by the Stewart phospholipid assay [37].

2.7. CF leakage assay

CF release from LUVs due to membrane permeation induced by the peptide was monitored at 37 °C by the fluorescence increase (excitation = 488 nm; emission = 520 nm). A concentration of lipid vesicles of 200 μM was used and CF leakage after peptide addition at 20 μM was monitored for 30 min. Complete dye release was obtained using 0.1% Triton X-100, which causes total destruction of lipid vesicles [38, 39]. The percentage of CF leakage was calculated according to the following formula [40]: leakage (%) = 100(F1 – F0)/(Ft – F0), where F0 represents the fluorescence of intact vesicles, and F1 and Ft denote the intensities of the fluorescence achieved by peptide and Triton X-100 treatment, respectively, at different time points, as indicated. The experiments were performed in duplicate and repeated three times.

2.8. Circular dichroism spectroscopy

In order to investigate the change in secondary structure of Esc(1-21) and Esc(1-21)-1c in SDS and DPC micelles, circular dichroism (CD) experiments were achieved using a Jasco J-815 spectrometer (Jasco International Co., Ltd. Tokyo, Japan) with a Peltier cell holder and temperature controller unit accessory. CD spectra were recorded for both the peptides in water (25 μM) and in the presence of different concentrations of SDS (peptide 25 μM, detergent 40 mM), DPC (peptide 25 μM, detergent 10 mM) at 37 °C, or in liposomes of POPE/POPG 7:3 (mol/mol) (peptide 5 or 20 μM, lipids up to 1 mM), at 25 °C. Both working concentrations of SDS and DPC micelles were above their critical micelle concentration (CMC) from previous literature [41]. The far-UV spectra were scanned over a range of 190-260 nm with 1 nm data interval and averaging over 4 scans. Blank sample spectra were subtracted from the raw data and the CD values were converted to per residue molar ellipticity ([θ]) (deg cm^2 $dmol^{-1}$).

2.9. Solution-state NMR experiments

All solution-state NMR experiments were executed on a Bruker Avance III 700 MHz spectrometer furnished with a CryoProbe at 310 K and/or 335 K. Topspin 3.1 (Bruker Biospin, Rheinstetten, Germany) and SPARKY 3.113 (UCSF) was used for processing and analysis of NMR data [42]. Two-dimensional total correlation (TOCSY) and nuclear Overhauser effect (NOESY) spectra of Esc(1-21) and Esc(1-21)-1c alone (1 mM) and in the presence of perdeuterated d_{25}-SDS (200 mM) and d_{38}-DPC (125 mM) were performed in aqueous solution comprising 10% D2O (pH ~4.5). All spectra were acquired at 1024 and 512 complex data points along t_2 and t_1 dimensions, respectively, where the States-TPPI-mode was used for quadrature detection in the t_1 dimension [43]. The spectral width was 12 ppm, the offset was adjusted at the water resonance (4.703 ppm) and the relaxation delay was of 2.0 s. TOCSY spectra were acquired using the standard pulse sequence of the pulse sequence library of the Bruker spectrometer, having excitation sculpting for water suppression and spin-lock mixing times of 80 ms (using MLEV-17 mixing scheme), whereas NOESY experiments with 80, 100, 150 and 250 ms mixing time were performed. Sequence-specific resonance assignment was accomplished based on 2D TOCSY and NOESY spectra of peptides in DPC micelles by means of standard assignment procedures [44]. All ^{1}H chemical shifts were referenced using DSS (2,2-Dimethyl-2-silapentane-5-sulfonate sodium salt) as an internal standard.

2.10. NMR derived structure calculation

The three-dimensional solution NMR structures of Esc(1-21) and Esc(1-21)-1c in DPC micelles were determined using the CYANA 2.1 software [45]. From NOESY spectra of Esc(1-21) and Esc(1-21)-1c in SDS and DPC micelles, NOE cross peak intensities were converted to upper bound distance limits of 3.0, 4.0, and 5.5 Å, corresponding to strong, medium, and weak intensities, respectively. The lower limits for all distance restraints were kept at 2.0 Å. In addition, the dihedral angle constraints were estimated from PREDITOR by means of $C^{\alpha}H$ chemical shifts and were used for structure calculations with ±20° variation, from the derived dihedral angle values [46]. Several

rounds of structure calculation were performed for iterative refinement using the standard protocol of CYANA 2.1, as described previously [47, 48]. Finally, the best 20 structures with lowest target function values were selected, depending upon low RMSD and minimum violation of distance and dihedral angle constraint. The stereochemical nature of the final structures was analyzed using PROCHECK-NMR validation suite [49]. To estimate the convergence of NMR-derived ensemble of structures, NH order parameters (S^2) [50] for both the peptides were calculated.

2.11. Preparation of peptide-loaded liposomes for solid-state NMR spectroscopy

Multilamellar vesicles (MLVs) were prepared by co-solubilization of lipids [POPE:POPE-$^2H_{31}$:POPG (2:1:1)] and peptides at the appropriate lipid-to-peptide ratio in chloroform/methanol 2:1 (v/v) to ensure homogenous mixing of the components, followed by solvent evaporation under a stream of nitrogen gas, removal of solvent traces by lyophilisation from a water suspension and then rehydration at h=0.9 [h = mass of water over the total mass of the system (phospholipids and water)]. To improve sample homogeneity the liposomes were repeatedly vortexed for 40 seconds, frozen in liquid nitrogen for 30 s and heated in a water bath at 40 °C for 10 min. After 1 to 3 freeze-thaw-vortex cycles, Esc(1-21) and Esc(1-21)-1c embedded in liposomes were obtained.

2.12. Solid-state NMR spectroscopy

^{2}H quadrupole echo experiments [51, 52] were acquired with a spectral width of 100 kHz, a recycle delay of 1 s, 25 μs echo delay, 30 ms acquisition time, π/2 pulses of 3.4 μs, and between 50k and 80k scans. All samples were investigated at temperatures at least 15K above the phase transition of the individual lipids of the mixture.

Oriented ^{2}H spectra were obtained from the powder pattern by de-Pakeing [53] thus the splitting can be measured more easily. The de-Paking procedure was performed according to the fast Fourier

transform-based deconvolution algorithm [54] and first spectral moments were calculated using the NMR-Depaker software (available from the Launchpad Web site: https://launchpad.net/nmr-friend).

Individual C–^{2}H bond order parameters ($S_{CD}i$) were calculated from quadrupolar splittings as described previously [52, 55],

$S_{CD}=4\Delta\nu_Q/3A_Q$ Eq. (1)

where A_Q is 167 KHz.

2.13. Average acyl chain length measurement

Calculation of acyl chain length is performed according to Douliez et al [56-60] and can be performed by considering the average projection of each C-C bond along the bilayer normal. This is achieved by connecting the S_{CD} order parameter to the C-C bonds order parameters (S_{CC}), and to sum all the average lengths of the aliphatic chain C-C bonds, projected on the normal to the bilayer. The average length of an aliphatic chain with an even number of carbons is obtained by the following expression:

$$\langle Lchain\rangle=\frac{1+\sqrt{1+8S_{mol}}}{4}\left[\langle l_{C_n-D}\rangle+1{,}25\cdot\sum_{k=2}^{n}\left(\frac{1}{2}+\frac{S_k^{CC}}{S_{mol}}\right)\right]$$ Eq.(3),

where $\langle l_{C_n-D}\rangle$ represents the contribution of the terminal methyl C_n-^{2}H bond, and S_{mol} is the molecular order parameter (taking into account wobbling motions).

By taking n =14 for DMPC and DMPE and n=16 for POPC and POPE; S_{mol} = 1, $\langle l_{C_n-D}\rangle$ is estimated equal to 1,09cos (35,25°) Å = 0.81 Å, and the angle between the C_n-^{2}H bond and C_{nl}-C_n being 111° the equation reduces to:

$$\langle Lchain\rangle=\left[0.81+1{,}25\cdot\sum_{k=2}^{n}\left(\frac{1}{2}+S_k^{CC}\right)\right]$$ Eq. (4)

The order parameter S_{CC} can be obtained after considering a fast axial rotation of the methyl group around the C_{nl}-C_n bond; hence, S_{CC} is obtained from measured S_{CD} using the recurring equation

$S_n^{CC} + S_{n+1}^{CC} = -2S_n^{CD}$. The order parameter for the nth term can be obtained from:

$$S_n^{CD} = \frac{3cos^2(111°)-1}{2} S_n^{CC} \qquad \text{Eq. (5)}$$

The area per lipid A is determined according to de Planque *et al*., and Nagle [61, 62]:

$$A=2\ [27.6\ Å^2/\ (1.27\ (0.5 + S_P))] \qquad \text{Eq. (6)}$$

where Sp is the average order parameter of the plateau region (carbons 2–6).

2.14. Statistical analysis

Quantitative data were expressed as the mean ± standard deviation (SD). Statistical analysis was performed using Student's t test with the PRISM software (GraphPad, San Diego, CA). Differences were considered to be statistically significant for $p < 0.05$ and are indicated in the legend to figures.

3. Results

3.1. Cytoplasmic membrane perturbation.

The diastereomer Esc(1-21)-1c was previously found to display a potent killing activity against the planktonic form of reference and cystic fibrosis strains of *P. aeruginosa* [30]. However, this activity was less pronounced than that of the parent Esc(1-21), as proved by the corresponding minimal bactericidal concentration (MBC) causing 99.9 % reduction in the number of viable cells within 30 min, in PBS. This was 4 μM *versus* 1 μM of Esc(1-21) when tested against a bacterial cell density of 1 x 10^6 CFU/ml [30].

To assess whether this difference reflected a different perturbation of the cytoplasmic membrane of this pathogen by the two peptides, a Sytox Green assay was carried out on two different bacterial strains: the reference *P. aeruginosa* PAO1 and the clinical isolate *P. aeruginosa* AA43. Sytox Green is a membrane-impermeable probe whose fluorescence intensity rapidly enhances upon binding to nucleic acids of bacterial cells with damaged cytoplasmic membrane; and its fluorescent signal is positively correlated to the level of membrane injury. Note that a significantly higher

number of bacterial cells (i.e. 1x 10^7 CFU/ml) than that generally used for *in vitro* antimicrobial assays is needed, in order to get a detectable signal [29]. As reported in Fig. 1 for *P. aeruginosa* AA43, both peptides were able to destabilize the bacterial membrane, but with a higher potency and faster kinetics for Esc(1-21) (see also the dose-response relationship after 5 min from peptide addition in the Supplementary Fig. S1). While almost total membrane perturbation was achieved by Esc(1-21) within 5 min (at the concentrations of 16 μM and 32 μM, Fig. 1 and Fig. S1) or 15 min (in the concentration range from 2 μM to 8 μM, Fig. 1), a significantly weaker and slower effect was recorded for Esc(1-21)-1c (Figs. 1 and S1). With reference to the latter, ~40% of membrane damage was caused at the highest peptide concentrations of 32 μM within 5 min (Fig. S1). The degree of membrane injury gradually diminished in a dose-dependent manner and became negligible at 1 μM. Differently, ~40% of membrane perturbation was registered at 1 μM of Esc(1-21) at the same time point of 5 min (Fig. S1). Similar results were also found for the reference PAO1 [29] and ATCC 27853 strains (data not shown). These data indicate a significant discrepancy between the two peptides in perturbing the cytoplasmic membrane of intact bacterial cells (i.e. much more than the 4 times ratio observed for the MBC values).

3.2. Activity on spheroplasts of P. aeruginosa

To investigate whether the bacterial cell wall was a barrier that differently interferes with the activity of the two peptides, their effect on *Pseudomonas* cells lacking of cell wall (i.e. spheroplasts) was studied. The reference strain of *P. aeruginosa* PAO1 was employed for this purpose and the peptides' effect on the viability of its spheroplasts (1 x 10^8 cells/ml) was evaluated by the MTT assay, 30 min after peptide addition at different concentrations, with respect to untreated control cells. As shown in Fig. 2, the percentage of metabolically-active spheroplasts after incubation with the all-L peptide at 2 μM was about 70%, while it dropped down to ~2% at 10 μM, in a dose-dependent manner. In comparison, the activity of the diastereomer on spheroplasts was lower, but

the difference was much lower than what was observed on intact cells: Esc(1-21)-1c was only ~ 1.5-fold less effective, with an LD_{50} of 4.4±0.5 μM *versus* 2.9 ± 0.5 μM of Esc(1-21).

3.3. Peptides' effect on LUVs of different composition

To expand our knowledge on the membrane perturbing activities of Esc(1-21) and Esc(1-21)-1c, the leakage of CF entrapped in the water volume inside liposomes made of both anionic and zwitterionic phospholipid bilayers was evaluated. A CF concentration of 30 mM was used to induce self-association and the consequent quenching of the dye [63]. After peptide administration, the membrane destabilization leads to probe release and dissociation with a resulting fluorescence increase. Both peptides were tested at a concentration of 20 μM on POPE/POPG liposomes (7:3 mol:mol, 200 μM), which mimic the lipid composition of the anionic membrane of Gram-negative bacteria. After addition to the lipid vesicles, Esc(1-21) gave rise to a 2-fold higher membrane-perturbing activity than the diastereomer, within 30 min (Fig. 3 panel A) and this was consistent with the results on spheroplasts.

When the two isomers were used on zwitterionic liposomes made of POPC/cholesterol (1:1, mol:mol) to simulate the neutral membrane of mammalian cells, a 5-fold lower leakage of entrapped CF was found for the diastereomer in comparison with its all-L counterpart (Fig. 3 panel B) in line with the lower cytotoxicity of Esc(1-21)-1c on mammalian cells [30, 32].

3.4. Structural studies by CD and NMR spectroscopy

In parallel, studies aimed at understanding the structural properties of the two peptides were performed by CD and multidimensional solution-state NMR spectroscopy, in the presence of micellar and liposomal membrane mimetics.

3.4.1. CD

The secondary structure of Esc(1-21) and Esc(1-21)-1c in membranes, and their affinity for lipid bilayers, was initially characterized by CD spectroscopy, in the presence of increasing concentrations of POPE/POPG liposomes (Fig.4). Their spectra presented a single negative minimum around 200 nm, a characteristic spectral signature for random coil conformations. By contrast, after addition of increasing concentrations of vesicles, the appearance of two negative minima at 208 nm and 222 nm was indicative of α-helical conformations of both peptide isomers, although to a lesser extent in the case of Esc(1-21)-1c (Fig. 4, panels A and B). The change in CD intensity at a fixed wavelength upon binding is directly proportional to the amount of complex formed.

$$[\theta]([L]) = [\theta]_{free} + \left([\theta]_{bound} - [\theta]_{free}\right) \cdot f_{bound}$$

Here, $[\theta]([L])$, $[\theta]_{free}$ and $[\theta]_{bound}$ are the values of molar ellipticity (in our case at 222 nm) observed at a given lipid concentration $[L]$, in the absence of liposomes, and in the completely bound state, respectively, and f_{bound} is the fraction of membrane-bound peptide [64].

In an ideal water-membrane partition equilibrium, f_{bound} depends on lipid concentration according to the following equation, where K_p is an apparent partition constant [63].

$$f_{bound} = \left(\frac{{}^{[L]}/_{K_p}}{1 + {}^{[L]}/_{K_p}} \right)$$

Combining these two equations, the expected lipid dependence of the molar ellipticity is given by

$$[\theta]([L]) = [\theta]_{free} + \left([\theta]_{bound} - [\theta]_{free}\right) \cdot \left(\frac{{}^{[L]}/_{K_p}}{1 + {}^{[L]}/_{K_p}} \right)$$

In our case, unfortunately, significant binding (and increase in helicity) took place only at lipid concentrations in the 100 μM range (Fig. 4 panels C and D), so that in the experimentally useful range of lipid concentrations (limited to 1 mM by the necessity to avoid scattering artefacts [65]) a plateau was not observed. For this reason, data fitting with the above equation was affected by a large uncertainty on the values of $[\theta]_{bound}$, and thus of K_p. However, the data are sufficient to indicate that the latter constant is of the same order of magnitude for the two peptides (~1 mM), although its value is possibly higher for Esc(1-21)-1c (blue lines).

In order to characterize the conformation of the two peptides when associated to a membrane-mimicking environment, CD spectra were measured in the presence of SDS (broken line) and DPC micelles (solid line), mimicking the anionic and zwitterionic composition of the outer leaflet of the cell membrane of bacteria and mammalian cells, respectively (Fig. 4, panels E, F). In this case, the smaller size of the amphiphilic aggregates reduced light scattering effects, compared to studies in the presence of vesicles. Therefore, surfactant concentrations much higher than the K_p values estimated for POPE/POPG liposomes could be employed, thus favouring peptide association to the micelles. In all cases, the spectral intensities typical of alpha helices were observed, although this was less pronounced in the case of Esc(1-21)-1c (Fig. 4 panel F), probably as a consequence of the presence of D-amino acids. The spectra in SDS exhibited a 222 nm intensity that is more negative than the 208 nm peaks. This finding is often considered indicative of the formation of helical aggregates [66].

3.4.2. NMR studies of Esc(1-21) and Esc(1-21)-1c in SDS and DPC micelles

The conformational transition from random coil to α-helical in the presence of membrane-mimicking environments, as detected by CD spectra, motivated us to explore the peptide structures at atomistic detail by high-resolution solution state NMR spectroscopy. DPC and/or SDS assemble as small size detergent micelles which, in contrast to large liposomes, provide appropriate systems

for the structural analysis of AMPs in membrane mimetic environments by multidimensional NMR spectroscopy, due to fast tumbling of the peptide-micellar complex in solution [67, 68].

Fig. 5 shows the amide proton region of the one-dimensional ^{1}H NMR spectra of Esc(1-21) and Esc(1-21)-1c in water and in the presence of SDS and DPC micelles. In water, both peptides displayed little dispersion and broad signals in the amide proton region of the spectra whereas in the presence of zwitterionic DPC micelles the spectra were not only well dispersed but also well resolved. The difference in one-dimensional proton spectral pattern demonstrated that micelles induced conformational transformation of both peptides with well-defined secondary structure. Moreover, in the presence of DPC micelles the spectra were better dispersed when compared to their association with SDS micelles, which can be accounted as differential conformational stabilization in the different micellar environment. Unfortunately, due to poor spectral resolution, in SDS micelles for both peptides extensive peak overlap in the fingerprint region of two-dimensional ^{1}H-^{1}H NOESY and TOCSY precludes further analysis of the 2D spectra.

With the help of two-dimensional ^{1}H-^{1}H TOCSY and NOESY spectra, sequential resonance assignment of Esc(1-21) and Esc(1-21)-1c in DPC was performed. It is noteworthy that the NOESY spectra in DPC micelles contained the adequate number of sequential and medium-range NOE cross peaks in comparison to the spectra in aqueous solution (Fig. S2 in SI). Therefore, the lack of diagnostic NOEs for both peptides in aqueous solution confirmed the CD spectral analysis where random coil conformations were observed. Differently, in zwitterionic DPC micelles the peptides adopted a more ordered conformation, as reported below. Intense sequential CαH/HN (i to i+1) NOEs were observed for all residues of both peptides (Fig. 6A and B). In addition, several medium range CαH/HN (i to i+2/i+3/i+4) NOEs were observed for Esc(1-21) throughout the peptide (Fig. S2 A and Fig. 6A). Furthermore, the presence of medium range NH/NH (i to i+2) NOE contacts reinforced the α-helical conformation of Esc(1-21). Overall the distribution of medium range CαH/HN (i to i+3/i+4) as well as NH/NH (i to i+2) backbone NOEs throughout the sequence

established an α-helical conformation in DPC micelles for Esc(1-21), in good accordance with the CD spectral analysis.

On the other hand, Esc(1-21)-1c in DPC micelles contained less diagnostic CαH/HN (i to i+2/i+3/i+4) NOEs in comparison to Esc(1-21) (Fig. S2 B). Most of the medium range NOEs (i to i+2/i+3/i+4) were observed in the N-terminal G1-N13 region (Fig. 6B). This was also in agreement with the trend in backbone NH/NH (i to i+2) NOE patterns which showed that most NOEs are in the N terminal region such as I2/F4, F3/K5, S4/L6, K5/A7 while the C-terminal stretch, having D-amino acid mutations at 14^{th} and 17^{th} position contained very few NOEs such as K12/L14, N13/L15 and I16/G18.

The discrepancy in NOE distribution for both peptides indicated that the N-terminal portion was mostly well-organized in the parent peptide while the C-terminal region of Esc(1-21)-1c was relatively unstructured and flexible in zwitterionic DPC micellar environments. This was supported by the trend in the ΔH^{α} values for each residue of Esc(1-21) and Esc(1-21)-1c where the chemical shift deviation of the alpha proton resonances from the reported values of random coil resonances provided information about the secondary structure of the peptide [69]. Here, a helical segment is characteristic of negative chemical shift deviation of ΔH^{α} for consecutive 4 residues while a positive chemical shift deviation is a signature of the beta sheet structure. In our systems in DPC micelles, all the CαH resonances throughout the sequence of Esc(1-21) and Esc(1-21)-1c experienced a downfield trend for the CαH chemical shifts (Fig. S3). This chemical shift deviation is a signature of the predominance of α-helical conformations in DPC micelles. Moreover, it was noted that the overall average chemical shift deviation was little higher in case of Esc(1-21) in comparison to Esc(1-21)-1c. The difference in average chemical shift deviation in the L14-G21 region was almost double for Esc(1-21) in comparison to Esc(1-21)-1c in line with the previous observation from NOESY spectra of both peptides.

3.5. Structure calculations for Esc(1-21) and Esc(1-21)-1c in DPC micelles

The NOESY derived distance constraints in conjunction with angular constrains, obtained from PREDITOR, were used to elucidate the three-dimensional conformations of Esc(1-21) and Esc(1-21)-1c peptides in DPC micellar solution. For structure calculations of Esc(1-21), a total of 190 distance restraints including 38 intra-residue, 85 sequential and 67 medium range constraints were used while in the case of Esc(1-21)-1c 39 intra-residue, 82 sequential and 44 medium range constraints (as a total of 165 NOEs) were available (Table 1). It is also evident that the number of medium range NOE constraints (i to i+2/i+3/i+4) was much less for Esc(1-21)-1c compared to Esc(1-21), which is also reflected in the RMSD from the ensemble of the 20 lowest energy structures, as reported below. The Esc(1-21) conformations converged to a helical structure extending from I2 to G21 with an average root mean square deviation (RMSD) for the backbone atoms (N, Cα, and C′) and the heavy atoms of 0.31 ± 0.13 and 0.67 ± 0.14 Å, respectively. On the other hand, the ensemble of conformations of Esc(1-21)-1c was not precise and diverged in the C-terminal as designated by RMSD values of 0.96 ± 0.20 and 1.28 ± 0.21 Å for backbone and heavy atoms, respectively. From the Ramachandran plot, it was seen that the backbone dihedral angles (Φ, Ψ) were accumulated in the most favoured regions for most of the residues of both Esc(1-21) and Esc(1-21)-lc, respectively.

In DPC micelles, Esc(1-21) adopted mainly α-helical conformations with a tilt at the N-terminal end (Fig. 7 A and B), whereas the central region of the α-helix was straight and amphipathic due to the presence of several polar residues such as K5, K9, K10, N13 and K20, across the one face of the helix. In contrast, the other face of the helix consists of the hydrophobic residues I2, F3, L6, A7, I11, L14, L15, I16 and L19. In the N terminal region of Esc(1-21), I2, F3 and L6 were in close vicinity; thereby facilitating CH_3-π interaction among β-branched side chains and the phenyl ring of the respective residues. Collectively, the amphipathicity of Esc(1-21) was conserved in its structure so that the cumulative hydrophobic and hydrophilic interactions governed the peptide stabilization

in DPC micelles. The amphipathic character was also obvious from a representation emphasizing the separation of hydrophobic and hydrophilic residues on opposite sides of the helix. (Fig. 7C).

In contrast, Esc(1-21)-1c in DPC micelles exhibits a partial α-helical conformation only at the N-terminal region between residues I2-N13, with an average backbone RMSD of 0.08 ± 0.02 (Fig. 8). However, the helix breaks after residue N13, likely due to the presence of two D-amino acids ^{D}L14 and ^{D}S17 [70]. It is also worth mentioning that the polar residues K5, K9 and K12 of Esc(1-21)-1c are located on one face of the N-terminal helical region, while the non-polar residues I2, F3, L6, A7 and I11 are on the opposite face of the helix, thereby maintaining an amphipathic character. Therefore, in comparison to Esc(1-21), Esc(1-21)-lc adopts a partial helical conformation only at the N-terminal region (G1-K12) while the C-terminal region (N13-G21) is unstructured and adopts a flexible conformation, which is well supported by the trend in N-H order (S^2) parameter for both peptides (Fig. S3). An order parameter of ~0.8 designates a well-defined backbone conformation, while smaller values indicate disordered backbone conformations. Both peptides exhibited similar trends in the order parameters of the (G1-K12) region, which are almost overlapping. The high order parameters indicate formation of well-defined backbone conformations for both Esc(1-21) and Esc(1-21)-1c. However, due to the incorporation of D-amino acids in the C-terminal part of Esc(1-21)-1c, the order parameter fluctuates in the (N13-G21) segment which supports the existence of poorly defined backbone conformations (Fig. S4). Collectively, close inspection suggests that the main difference between both the structures are in the C-terminal region L14-G21 (Fig. 9).

3.6. Membrane disorder induced by both Esc(1-21) and Esc(1-21)-1c

To gain insight into how membrane insertion of these amphiphilic peptides changes the fatty acyl chain packing of phospholipid bilayers, solid-state ^{2}H-NMR spectra of membranes encompassing 75 mole % of POPE and 25 mole % of PG lipid were recorded. To assess how the lipid chain

mobility and the conformational distribution of the methylene segments is influenced by Esc(1-21) or its diastereomer, the quadrupolar splittings of the ^{2}H-NMR spectra were recorded and converted into order parameter profiles. The corresponding order parameter profiles of POPE-d_{31} are shown in Fig. 10 and display the characteristic signature of bilayer packing, with a plateau of $|S_{CD}|$ values extending towards the 6th carbon position. The plateau regions exhibit a value of ca. 0.23 for the pure lipid system and of ca. 0.21 for membrane embedded with Esc(1-21) or Esc(1-21)-1c. In both cases, the chain order of the POPE palmitoyl was found to be significantly reduced when compared to the pure lipid sample (Fig. 10). As outlined in the methods section, the ^{2}H NMR order parameters can be converted into the thickness of the acyl chain region of the bilayer ($<L_{chain}>$) and into the area per lipid (A) assuming that these values reflect the distribution of the acyl chain conformation. Therefore, one obtains $<L_{chain}>$ = 13.4 ±0.1 Å for the pure system and 13.1 ±0.1 Å upon addition of 2 mole % Esc(1-21) or Esc(1-21)-1c. Although the difference in average thickness may appear small, the membrane disordering effects in the direct vicinity of the peptides are probably more pronounced and the decreases in order parameters are significant.

4. Discussion

Recently, the short-sized AMP Esc(1-21) and especially its diastereomer Esc(1-21)-1c have been identified as encouraging candidates for the development of new anti-infective agents, because of their unique properties [30, 32]. The diastereomer showed a relevant bactericidal activity against the planktonic form of the bacterial pathogen *P. aeruginosa*, albeit ~4-fold lower than that of Esc(1-21). Here, to investigate the reasons accounting for this difference, the bacterial membrane perturbation was initially assessed by the Sytox Green assay on intact bacterial cells. Similarly to the bactericidal activity, but with a more pronounced difference between the two peptides, a stronger and faster membrane permeabilization was recorded for Esc(1-21). Therefore, it can be stated that the weaker *in vitro* antibacterial activity of Esc(1-21)-1c on the planktonic phenotype of

the Gram-negative bacterium *P. aeruginosa*, as compared to Esc(1-21) is mainly associated to a weaker ability in perturbing the bacterial membrane of this pathogen with consequent cell death. In general, such a difference can have three origins [71-73]: a) a different peptide ability in crossing the LPS outer layer and reaching the target bacterial membrane; b) a different affinity for the anionic bacterial membrane; c) differential effects once the peptides are bound to the phospholipid bilayers.

Interestingly, when the effect of the two peptides was tested on cells devoid of cell wall i.e. spheroplasts of *Pseudomonas* instead of whole bacterial cells, only a slightly more (1.5-fold) pronounced microbicidal activity was obtained for the wild-type Esc(1-21) with respect to the diastereomer. Similarly, when the two isomers were analysed on anionic model membranes, the all-L Esc(1-21) was found to induce ~ 2-fold higher leakage of vesicle contents in comparison to Esc(1-21)-1c. Indeed, CD studies indicated that the affinities of the two peptides for these membranes were only slightly different, while solid-state NMR studies revealed a similar effect of the two peptides on the membrane order parameters. Based on these observations, we can exclude that differences in the antibacterial activity between the two esculentin-derived peptides are mainly due to significant differences in their membrane affinity (hypothesis b) or to a different ability to affect the phospholipid bilayer of the cytoplasmic membrane once inserted into it (hypothesis c). By exclusion, we are led to conclude that the bactericidal activity of the diastereomer against planktonic *P. aeruginosa* cells, compared to the parent peptide, is significantly impaired by a different interaction with the cell wall components, including the LPS outer membrane, which is lacking in spheroplasts. This is in agreement with previous studies revealing that the relative binding affinity of Esc(1-21)-1c to *P. aeruginosa* LPS is ~ 8-fold lower in magnitude than Esc(1-21) binding to LPS and that a minor perturbation of LPS structure is caused by the diastereomer when compared to Esc(1-21) [48].

In this work we have also seen how replacement of two amino acids with the corresponding D-enantiomers in the C-terminal region of Esc(1-21) is sufficient to obtain a peptide, Esc(1-21)-1c, with a reduced α-helical content along with a lower tendency in perturbing zwitterionic model membranes. This is in line with its reduced effect on mammalian cells compared to the all-L peptide, as indicated by the corresponding concentrations causing 50% cell death (>256 μM in comparison to a LD_{50} ranging from 64 μM to 150 μM for the all-L peptide) [30]).

According to the literature, the ease of adopting stable amphipathic three-dimensional folds, which for many peptides is achieved by α–helix formation is an essential factor for AMPs to cause cytotoxicity [74, 75]. As demonstrated by solution NMR studies in DPC micelles which simulate the neutral membrane of mammalian cells, an α-helical structure is preserved along the entire amino acid sequence of Esc(1-21), while a highly flexible C-terminal arm is present in Esc(1-21)-1c. This is attributed to the presence of D-amino acids at 14^{th} and 17^{th} position, which break the stereo chemical integrity of the sequence made of L-amino acids. This corroborates well previous structural studies of naturally occurring AMPs e.g. magainin, cytolysin and melittin [76-78].

Interestingly, a remarkable structural difference was observed between the two peptides either in aggregates of LPS, the major component of the outer-membrane of Gram-negative bacteria or in DPC micelles mimicking the lipid composition of the mammalian cell membrane (Fig. S5). The main difference is at the C-terminal region (N13-G18) of Esc(1-21)-lc (Fig. S5 B and Table 1), whose higher flexibility (RMSD=0.96 ± 0.20 Å) (Table 1) may interfere with the peptide ability to destabilize bacterial and mammalian cell membranes in comparison to the parent Esc(1-21) [32] .

Importantly, even though the two amino acids substitutions was found to lead to a somewhat weaker activity of the peptide against free-living cells of *P. aeruginosa* [30], a higher potency was

shown by Esc(1-21)-1c against the more resistant form of *P. aeruginosa,* that is its biofilm community [30].

Note that the lower antimicrobial activity against the planktonic state of Pseudomonas is not in contradiction with its stronger effectiveness in killing the more dangerous biofilm phenotype [79]. Compared to the all-L peptide, Esc(1-21)-1c is more resistant to proteases which are mainly produced by cells within biofilms and much less by free living bacteria [80]. This may prolong the residence time of the diastereomer and therefore its exposure to the bacterial cells, resulting in a prolonged antimicrobial efficacy in comparison with the all-L peptide, which would be rapidly degraded. In addition, it has been lately demonstrated that D-amino acids can promote the disassembly of the extracellular matrix of biofilm cells [81, 82].

Finally, it is worthwhile recalling that the diastereomer showed a reduced cytotoxicity and anti-inflammatory activity [30] than the all-L peptide. This would represent an advantage for the host immune response to bacterial infection at the initial stage.

5. Conclusions

In this work we demonstrated how the cell wall of the free living form of *P. aeruginosa* plays a major role in determining differences in the antibacterial activity between the two esculentin isomers. Most likely, a weaker binding of the diastereomer Esc(1-21)-1c to LPS and presumably slower translocation into the target bacterial membrane account for its weaker activity in comparison to the all-L peptide. The slightly lower ability in binding and perturbing anionic phospholipid bilayers for Esc(1-21)-1c contributes only in a small part to this difference, while the final effect on membrane thinning once the peptide is inserted into the membrane is identical to that provoked by Esc(1-21).

Moreover, we showed how two L-to-D amino acid substitutions in Esc(1-21) led to a lower tendency in perturbing zwitterionic model membranes in line with the lower cytotoxicity of the diastereomer.

In summary, even if Esc(1-21)-1c has a weaker bactericidal activity than the all-L peptide against the planktonic form of Pseudomonas, this still occurs at a low micromolar range [30] and it comes with a significant higher peptide biostability, higher wound-healing activity, less pronounced cytotoxicity and anti-inflammatory property [30]. Overall, these findings represent a valuable compromise for the development of a safer antibacterial agent with an extended *in vivo* activity. This is supported by our recent *in vivo* efficacy studies on the two selected peptide isoforms [83].Finally, besides providing information on the structural organization of the two esculentin-derived AMPs, our data may assist in the design of new anti-infective agents with optimized biological properties.

Acknowledgments

This research was supported by Grants from Sapienza University of Rome (to M.L.M) and by Plan project-II, Bose Institute (to AB). Part of this work was also supported by the Italian Cystic Fibrosis Research Foundation (Project FFC#11/2014 adopted by FFC Delegations from Siena, Sondrio Valchiavenna, Cerea Il Sorriso di Jenny, and Pavia) (to M.L.M.).

The financial contributions of the Agence Nationale de la Recherche (projects MemPepSyn 14-CE34-0001-01 (to B.B.) and the LabEx Chemistry of Complex Systems 10-LABX-0026_CSC), the University of Strasbourg, the CNRS, the Région Alsace and the RTRA International Center of Frontier Research in Chemistry are gratefully acknowledged. M.L.M thanks Alessandra Bragonzi (San Raffaele Institute, Milan, Italy) and Burkhard Tummler (Klinische Forschergruppe, OE 6710, Medizinische Hochschule Hannover, Germany) for the *P. aeruginosa* clinical isolate.

AG thanks Bose Institute for fellowship. AB also would like to acknowledge DBT, Government of India, for infrastructure development fund (BT/PR3106/INF/22/138/2011) to Bose Institute for purchasing 700 MHz NMR spectrometer with cryoprobe. The calculated structure of the peptides in the presence of DPC was deposited in protein data bank (PDB) with pdb accession code PDB ID 5XDJ.LS acknowledges support by MIUR (grant PRIN 20157WW5EH_007) and Università di Roma "Tor Vergata" (Consolidate the Foundations grant AMPSA).

References

1 Y. Shai. Mode of action of membrane active antimicrobial peptides. Biopolymers. 66 (2002), 236-248

2 N. Mookherjee, R.E. Hancock. Cationic host defence peptides: innate immune regulatory peptides as a novel approach for treating infections. Cell Mol Life Sci. 64 (2007), 922-933

3 H.G. Boman. Peptide antibiotics and their role in innate immunity. Annu Rev Immunol. 13 (1995), 61-92

4 H. Jenssen, P. Hamill, R.E. Hancock. Peptide antimicrobial agents. Clin Microbiol Rev. 19 (2006), 491-511

5 R.M. Epand, H.J. Vogel. Diversity of antimicrobial peptides and their mechanisms of action. Biochim Biophys Acta. 1462 (1999), 11-28

6 R.F. Epand, M.A. Schmitt, S.H. Gellman, R.M. Epand. Role of membrane lipids in the mechanism of bacterial species selective toxicity by two alpha/beta-antimicrobial peptides. Biochim Biophys Acta. 1758 (2006), 1343-1350

7 R.M. Epand, R.F. Epand. Bacterial membrane lipids in the action of antimicrobial agents. J Pept Sci. 17 (2011), 298-305

8 K.L. Piers, R.E. Hancock. The interaction of a recombinant cecropin/melittin hybrid peptide with the outer membrane of *Pseudomonas aeruginosa*. Mol Microbiol. 12 (1994), 951-958

9 M. Zasloff. Antimicrobial peptides of multicellular organisms. Nature. 415 (2002), 389-395

10 E.F. Haney, S. Nathoo, H.J. Vogel, E.J. Prenner. Induction of non-lamellar lipid phases by antimicrobial peptides: a potential link to mode of action. Chem Phys Lipids. 163 (2010), 82-93

11 K. Lohner, S.E. Blondelle. Molecular mechanisms of membrane perturbation by antimicrobial peptides and the use of biophysical studies in the design of novel peptide antibiotics. Comb Chem High Throughput Screen. 8 (2005), 241-256

12 K.A. Brogden. Antimicrobial peptides: pore formers or metabolic inhibitors in bacteria? Nat Rev Microbiol. 3 (2005), 238-250

13 A. Ghosh, R.K. Kar, J. Jana, A. Saha, B. Jana, J. Krishnamoorthy, D. Kumar, S. Ghosh, S. Chatterjee, A. Bhunia. Indolicidin targets duplex DNA: structural and mechanistic insight through a combination of spectroscopy and microscopy. ChemMedChem. 9 (2014), 2052-2058

14 H. Bai, Y. Zhou, Z. Hou, X. Xue, J. Meng, X. Luo. Targeting bacterial RNA polymerase: promises for future antisense antibiotics development. Infect Disord Drug Targets. 11 (2011), 175-187

15 J.K. Savjani, A.K. Gajjar, K.T. Savjani. Mechanisms of resistance: useful tool to design antibacterial agents for drug - resistant bacteria. Mini Rev Med Chem. 9 (2009), 194-205

16 Y. Carmeli, N. Troillet, G.M. Eliopoulos, M.H. Samore. Emergence of antibiotic-resistant *Pseudomonas aeruginosa*: comparison of risks associated with different antipseudomonal agents. Antimicrob Agents Chemother. 43 (1999), 1379-1382

17 K. Lohner. Membrane-active antimicrobial peptides as template structures for novel antibiotic agents. Curr Top Med Chem 17 (2017), 508-519

18 A.P. Magiorakos, A. Srinivasan, R.B. Carey, Y. Carmeli, M.E. Falagas, C.G. Giske, S. Harbarth, J.F. Hindler, G. Kahlmeter, B. Olsson-Liljequist, D.L. Paterson, L.B. Rice, J. Stelling, M.J. Struelens, A. Vatopoulos, J.T. Weber, D.L. Monnet. Multidrug-resistant, extensively drug-resistant and pandrug-resistant bacteria: an international expert proposal for interim standard definitions for acquired resistance. Clin Microbiol Infect. 18 (2012), 268-281

19 M.L. Mangoni. Host-defense peptides: from biology to therapeutic strategies. Cell Mol Life Sci. 68 (2011), 2157-2159

20 C.R. Lee, I.H. Cho, B.C. Jeong,S.H. Lee. Strategies to minimize antibiotic resistance. Int J Environ Res Public Health. 10 (2013), 4274-4305

21 A. Nigam, D. Gupta, A. Sharma. Treatment of infectious disease: beyond antibiotics. Microbiol Res. 169 (2014), 643-651

22 D.K. Mercer, D.A. O'Neil. Peptides as the next generation of anti-infectives. Future Med Chem. 5 (2013), 315-337

23 K. Fosgerau,T. Hoffmann. Peptide therapeutics: current status and future directions. Drug Discov Today. 20 (2015), 122-128

24 A.A. Kaspar, J.M. Reichert. Future directions for peptide therapeutics development. Drug Discov Today. 18 (2013), 807-817

25 P. Kosikowska, A. Lesner. Antimicrobial peptides (AMPs) as drug candidates: a patent review (2003-2015). Expert Opin Ther Pat. 26 (2016), 689-702

26 A.E. Islas-Rodriguez, L. Marcellini, B. Orioni, D. Barra, L. Stella,M.L. Mangoni. Esculentin 1-21: a linear antimicrobial peptide from frog skin with inhibitory effect on bovine mastitis-causing bacteria. J Pept Sci. 15 (2009), 607-614

27 T. Gamberi, D. Cavalieri, F. Magherini, M.L. Mangoni, C. De Filippo, M. Borro, G. Gentile, M. Simmaco, A. Modesti. An integrated analysis of the effects of Esculentin 1-21 on *Saccharomyces cerevisiae*. Biochim Biophys Acta. 1774 (2007), 688-700

28 M.L. Mangoni, V. Luca, A.M. McDermott. Fighting microbial infections: A lesson from amphibian skin-derived esculentin-1 peptides. Peptides 71 (2015), 286-295

29 V. Luca, A. Stringaro, M. Colone, A. Pini,M.L. Mangoni. Esculentin(1-21), an amphibian skin membrane-active peptide with potent activity on both planktonic and biofilm cells of the bacterial pathogen *Pseudomonas aeruginosa*. Cell Mol Life Sci. 70 (2013), 2773-2786

30 A. Di Grazia, F. Cappiello, H. Cohen, B. Casciaro, V. Luca, A. Pini, Y.P. Di, Y. Shai,M.L. Mangoni. D-Amino acids incorporation in the frog skin-derived peptide esculentin-1a(1-21)NH is beneficial for its multiple functions. Amino Acids 47 (2015), 2505-2519

31 A. Di Grazia, F. Cappiello, A. Imanishi, A. Mastrofrancesco, M. Picardo, R. Paus,M.L. Mangoni. The frog skin-derived antimicrobial peptide esculentin-1a(1-21)NH2 promotes the migration of human HaCaT keratinocytes in an EGF receptor-dependent manner: a novel promoter of human skin wound healing? PLoS One. 10 (2015), e0128663

32 F. Cappiello, A. Di Grazia, L.A. Segev-Zarko, S. Scali, L. Ferrera, L. Galietta, A. Pini, Y. Shai, Y.P. Di,M.L. Mangoni. Esculentin-1a-derived peptides promote clearance of *Pseudomonas aeruginosa* internalized in bronchial cells of cystic fibrosis patients and lung cell migration: biochemical properties and a plausible mode of action. Antimicrob Agents Chemother. 60 (2016), 7252-7262

33 A. Bragonzi, M. Paroni, A. Nonis, N. Cramer, S. Montanari, J. Rejman, C. Di Serio, G. Doring,B. Tummler. *Pseudomonas aeruginosa* microevolution during cystic fibrosis lung infection establishes clones with adapted virulence. Am J Respir Crit Care Med. 180 (2009), 138-145

34 C.J. Sullivan, J.L. Morrell, D.P. Allison,M.J. Doktycz. Mounting of *Escherichia coli* spheroplasts for AFM imaging. Ultramicroscopy. 105 (2005), 96-102

35 D. Uccelletti, E. Zanni, L. Marcellini, C. Palleschi, D. Barra, M.L. Mangoni. Anti-Pseudomonas activity of frog skin antimicrobial peptides in a *Caenorhabditis elegans* infection model: a plausible mode of action *in vitro* and *in vivo.* Antimicrob Agents Chemother. 54 (2010), 3853-3860

36 S.M. Kelly, T.J. Jess,N.C. Price. How to study proteins by circular dichroism. Biochim Biophys Acta. 1751 (2005), 119-139

37 J.C. Stewart. Colorimetric determination of phospholipids with ammonium ferrothiocyanate. Anal Biochem. 104 (1980), 10-14

38 L. Marcellini, M. Borro, G. Gentile, A.C. Rinaldi, L. Stella, P. Aimola, D. Barra,M.L. Mangoni. Esculentin-1b(1-18)--a membrane-active antimicrobial peptide that synergizes with antibiotics and modifies the expression level of a limited number of proteins in *Escherichia coli.* FEBS J. 276 (2009), 5647-5664

39 A. Makovitzki, D. Avrahami,Y. Shai. Ultrashort antibacterial and antifungal lipopeptides. Proc Natl Acad Sci U S A. 103 (2006), 15997-16002

40 K. Matsuzaki. Why and how are peptide-lipid interactions utilized for self-defense? Magainins and tachyplesins as archetypes. Biochim Biophys Acta. 1462 (1999), 1-10

41 G. Manzo, M. Carboni, A.C. Rinaldi, M. Casu,M.A. Scorciapino. Characterization of sodium dodecylsulphate and dodecylphosphocholine mixed micelles through NMR and dynamic light scattering. Magn Reson Chem. 51 (2013), 176-183

42 T. Goddard, and D. G. Kneller. SPARKY 3." University of California, San Francisco. 14 (2004), 15

43 M. Piotto, V. Saudek,V. Sklenar. Gradient-tailored excitation for single-quantum NMR spectroscopy of aqueous solutions. J Biomol NMR. 2 (1992), 661-665

44 K. Wuthrich. NMR of proteins and nucleic acids. Wiley (1986)

45 P. Guntert, C. Mumenthaler,K. Wuthrich. Torsion angle dynamics for NMR structure calculation with the new program DYANA. J Mol Biol. 273 (1997), 283-298

46 M.V. Berjanskii, S. Neal,D.S. Wishart. PREDITOR: a web server for predicting protein torsion angle restraints. Nucleic Acids Res. 34 (2006), W63-69

47 A. Datta, A. Ghosh, C. Airoldi, P. Sperandeo, K.H. Mroue, J. Jimenez-Barbero, P. Kundu, A. Ramamoorthy,A. Bhunia. Antimicrobial peptides: insights into membrane permeabilization, lipopolysaccharide fragmentation and application in plant disease control. Sci Rep. 5 (2015), 11951

48 A. Ghosh, S. Bera, Y. Shai, M.L. Mangoni,A. Bhunia. NMR structure and binding of esculentin-1a (1-21)NH2 and its diastereomer to lipopolysaccharide: Correlation with biological functions. Biochim Biophys Acta. 1858 (2016), 800-812

49 R.A. Laskowski, J.A. Rullmannn, M.W. MacArthur, R. Kaptein,J.M. Thornton. AQUA and PROCHECK-NMR: programs for checking the quality of protein structures solved by NMR. J Biomol NMR. 8 (1996), 477-486

50 F. Zhang,R. Bruschweiler. Contact model for the prediction of NMR N-H order parameters in globular proteins. J Am Chem Soc. 124 (2002), 12654-12655

51 J.H. Davis, K.R. Jeffrey, M. Bloom, M.I. Valic Quadrupolar echo deuteron magnetic resonance spectroscopy in ordered hydrocarbon chains. Chemical Physics Letters. 42 (1976), 390-394

52 J.H. Davis. The description of membrane lipid conformation, order and dynamics by 2H-NMR. Biochim Biophys Acta. 737 (1983), 117-171

53 M. Bloom, J.H. Davis, A.L. Mackay Mackay. Direct determination of the oriented sample NMR spectrum from the powder spectrum for the systems with local axial symmetry. Chem. Phys. Letters. 80 (1981), 198-202

54 M.A. McCabe,S.R. Wassall. Rapid deconvolution of NMR powder spectra by weighted fast Fourier transformation. Solid State Nucl Magn Reson. 10 (1997), 53-61

55 J. Seelig. Deuterium magnetic resonance: theory and application to lipid membranes. Q Rev Biophys. 10 (1977), 353-418

56 J.P. Douliez, A. Leonard,E.J. Dufourc. Restatement of order parameters in biomembranes: calculation of C-C bond order parameters from C-D quadrupolar splittings. Biophys J. 68 (1995), 1727-1739

57 L.A. Douliez Jean-Paul , Dufourc Erick J. Conformational order of DMPC sn-1 versus sn-2 chains and membrane thickness: an approach to molecular protrusion by solid state 2H-NMR and neutron diffraction. J.Chim.Phys. 100 (1996), 18450-18457

58 H. Schindler,J. Seelig. Deuterium order parameters in relation to thermodynamic properties of a phospholiped bilayer. A statistical mechanical interpretation. Biochemistry. 14 (1975), 2283-2287

59 S.L. Grage, S. Afonin, S. Kara, G. Buth,A.S. Ulrich. Membrane thinning and thickening induced by membrane-active amphipathic peptides. Front Cell Dev Biol. 4 (2016), 65

60 A. Grelard, P. Guichard, P. Bonnafous, S. Marco, O. Lambert, C. Manin, F. Ronzon,E.J. Dufourc. Hepatitis B subvirus particles display both a fluid bilayer membrane and a strong resistance to freeze drying: a study by solid-state NMR, light scattering, and cryo-electron microscopy/tomography. FASEB J. 27 (2013), 4316-4326

61 M.R. de Planque, D.V. Greathouse, R.E. Koeppe, 2nd, H. Schafer, D. Marsh,J.A. Killian. Influence of lipid/peptide hydrophobic mismatch on the thickness of diacylphosphatidylcholine bilayers. A 2H NMR and ESR study using designed transmembrane alpha-helical peptides and gramicidin A. Biochemistry. 37 (1998), 9333-9345

62 J.F. Nagle. Area/lipid of bilayers from NMR. Biophys J. 64 (1993), 1476-1481

63 L. Stella, C. Mazzuca, M. Venanzi, A. Palleschi, M. Didone, F. Formaggio, C. Toniolo,B. Pispisa. Aggregation and water-membrane partition as major determinants of the activity of the antibiotic peptide trichogin GA IV. Biophys J. 86 (2004), 936-945

64 G. Bocchinfuso, S. Bobone, C. Mazzuca, A. Palleschi,L. Stella. Fluorescence spectroscopy and molecular dynamics simulations in studies on the mechanism of membrane destabilization by antimicrobial peptides. Cell Mol Life Sci. 68 (2011), 2281-2301

65 A.S. Ladokhin, M. Fernandez-Vidal,S.H. White. CD spectroscopy of peptides and proteins bound to large unilamellar vesicles. J Membr Biol. 236 (2010), 247-253

66 S.Y. Lau, A.K. Taneja,R.S. Hodges. Synthesis of a model protein of defined secondary and quaternary structure. Effect of chain length on the stabilization and formation of two-stranded alpha-helical coiled-coils. J Biol Chem. 259 (1984), 13253-13261

67 L. Maler. Solution NMR studies of peptide-lipid interactions in model membranes. Mol Membr Biol. 29 (2012), 155-176

68 R. Wimmer,L.E. Uggerhoj. Determination of Structure and Micellar Interactions of Small Antimicrobial Peptides by Solution-State NMR. Methods Mol Biol. 1548 (2017), 73-88

69 D.S. Wishart, C.G. Bigam, J. Yao, F. Abildgaard, H.J. Dyson, E. Oldfield, J.L. Markley,B.D. Sykes. 1H, 13C and 15N chemical shift referencing in biomolecular NMR. J Biomol NMR. 6 (1995), 135-140

70 P.Y. Chou,G.D. Fasman. Empirical predictions of protein conformation. Annu Rev Biochem. 47 (1978), 251-276

71 M.L. Mangoni, R.F. Epand, Y. Rosenfeld, A. Peleg, D. Barra, R.M. Epand,Y. Shai. Lipopolysaccharide, a key molecule involved in the synergism between temporins in inhibiting bacterial growth and in endotoxin neutralization. J Biol Chem. 283 (2008), 22907-22917

72 D. Roversi, V. Luca, S. Aureli, Y. Park, M.L. Mangoni,L. Stella. How many antimicrobial peptide molecules kill a bacterium? The case of PMAP-23. ACS Chem Biol. 9 (2014), 2003-2007

73 F. Savini, V. Luca, A. Bocedi, R. Massoud, Y. Park, M.L. Mangoni,L. Stella. Cell-Density Dependence of Host-Defense Peptide Activity and Selectivity in the Presence of Host Cells. ACS Chem Biol. 12 (2017), 52-56

74 E. Gazit, W.J. Lee, P.T. Brey,Y. Shai. Mode of action of the antibacterial cecropin B2: a spectrofluorometric study. Biochemistry. 33 (1994), 10681-10692

75 Y. Pouny, D. Rapaport, A. Mor, P. Nicolas,Y. Shai. Interaction of antimicrobial dermaseptin and its fluorescently labeled analogues with phospholipid membranes. Biochemistry. 31 (1992), 12416-12423

76 Y. Shai,Z. Oren. Diastereoisomers of cytolysins, a novel class of potent antibacterial peptides. J Biol Chem. 271 (1996), 7305-7308

77 R. Saravanan, A. Bhunia,S. Bhattacharjya. Micelle-bound structures and dynamics of the hinge deleted analog of melittin and its diastereomer: implications in cell selective lysis by D-amino acid containing antimicrobial peptides. Biochim Biophys Acta. 1798 (2010), 128-139

78 T. Wieprecht, O. Apostolov, M. Beyermann,J. Seelig. Thermodynamics of the alpha-helix-coil transition of amphipathic peptides in a membrane environment: implications for the peptide-membrane binding equilibrium. J Mol Biol. 294 (1999), 785-794

79 E. Drenkard,F.M. Ausubel. Pseudomonas biofilm formation and antibiotic resistance are linked to phenotypic variation. Nature. 416 (2002), 740-743

80 G. Singh, B. Wu, M.S. Baek, A. Camargo, A. Nguyen, N.A. Slusher, R. Srinivasan, J.P. Wiener-Kronish,S.V. Lynch. Secretion of *Pseudomonas aeruginosa* type III cytotoxins is dependent on pseudomonas quinolone signal concentration. Microb Pathog. 49 (2010), 196-203

81 D. Romero, H. Vlamakis, R. Losick,R. Kolter. An accessory protein required for anchoring and assembly of amyloid fibres in B. subtilis biofilms. Mol Microbiol. 80 (2011), 1155-1168

82 L. Segev-Zarko, R. Saar-Dover, V. Brumfeld, M.L. Mangoni,Y. Shai. Mechanisms of biofilm inhibition and degradation by antimicrobial peptides. Biochem J. 468 (2015), 259-270

83. C. Chen C, M.L. Mangoni, Y.P. Di. *In vivo* therapeutic efficacy of frog skin-derived peptides against *Pseudomonas aeruginosa*-induced pulmonary infection. Sci Rep. 7 (2017), 8548

Table 1 summarizes the information for the 20 final NMR structures of Esc(1-21) and Esc(1-21)-1c in DPC micelles.

Distance restrains	Esc(1-21)	Esc(1-21)-lc
Intra-residue (i–j = 0)	38	39
Sequential (|i–j| = 1)	85	82
Medium-range (2≤|i–j|≤4)	67	44
Long-range (|i–j| ≥5)	0	0
Total	190	165
Angular restraints	40	40
Φ (phi)	20	20
Ψ (psi)	20	20
Distance restraints from violations (≥ 0.3Å)	0	1
Deviation from mean structure (Å) Average back bone to mean structure (G1-N13)	0.31 ± 0.13 0.08 ± 0.02	0.96 ± 0.20
Average heavy atom to mean structure	0.67 ± 0.14	1.28 ± 0.21
Ramachandran plot analysis for ensemble		
% Residues in the most favourable and additionally allowed regions	(98.4+1.6) =100	(90.0+6.6) =96.6
% Residues in the generously allowed Region	0	3.4
% Residues in the disallowed region	0	0

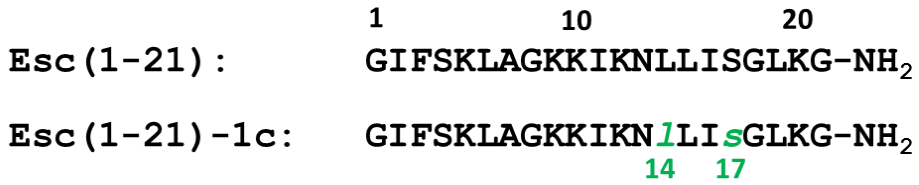

Scheme 1. Amino acid sequence of (A) Esc(1-21) and (B) Esc(1-21)-1c. The D-amino acids at position 14 and 17 are shown in green and in italics.

Figure legends

Fig. 1. Kinetics of cytoplasmic membrane permeabilization of the planktonic form of *P. aeruginosa* AA43. Cells (1×10^7 CFU/ml) were incubated with 1 μM Sytox Green in PBS. Once basal fluorescence reached a constant value, the peptide was added (*arrow*, $t = 0$) at different concentrations and changes in fluorescence (λ_{exc} = 485 nm, λ_{ems} = 535 nm) were monitored for 60 min and plotted as the percentage of membrane perturbation relative to that obtained after treating bacteria with the highest peptide concentration (32 μM) and the addition of 1 mM EDTA + 0.5 % Triton-X100. Data points represent the mean of triplicate samples from a single experiment, representative of three different experiments. Cells not exposed to the peptide were used as control (Ctrl).

Fig.2. Effect of different concentrations of Esc(1-21), red line, and its diastereomer , blue line, on the viability of spheroplasts of *P. aeruginosa* PAO1, 30 min after treatment at 37 °C. Cell viability was determined by the MTT reduction to insoluble formazan (see Materials and Methods) and is expressed as percentage with respect to the control (cells not treated with the peptide). Data represent the mean ± SD of three independent experiments performed in triplicate. The level of statistical significance between samples treated with Esc(1-21) and Esc(1-21)-1c are indicated as follows $*p < 0.05$, $***p < 0.001$

Fig. 3. CF release from POPE/POPG (panel A) and POPC/chol (panel B) LUVs (final lipid concentration 200 μM) within 30 min after addition of peptides (20 μM) at 37 °C. The percentage of leakage was calculated according to the formula: 100(Ft – F0) / (F1 – F0) as explained in the Materials and Methods. Data points are means ± SD of three independent measurements performed in duplicate. The difference between the two peptides was significant ($p< 0.05$) .

Fig. 4. Top row: Circular dichroism spectra of Esc(1-21) (panel A) and Esc(1-21)-1c (panel B), measured in the presence of increasing lipid concentrations (POPE/POPG 7/3, mol/mol). Peptide concentration: 20 μM, lipid concentrations: 1 μM, 2 μM, 5 μM, 10 μM, 20 μM, 50 μM, 100 μM, 200 μM, 500 μM and 1 mM. The CD spectra are colored from blue to red, in order of increasing concentrations and following the order of colors in the visible spectrum.

Middle row: Mean residue ellipticity ([θ]) values at 222 nm as function of lipid concentrations, [peptide]= 20 μM (panel C) and [peptide]= 5 μM (panel D), Esc(1-21) in red and Esc (1-21)-1c in blue.

Bottom row: Circular dichroism spectra of Esc(1-21) (panel E) and Esc(1-21)-1c (panel F), measured in the presence of SDS (broken line) and DPC (solid line) (25 μM peptide, 40 mM SDS or 10 mM DPC).

Fig. 5. Left Panel: Amide proton region of ^{1}H NMR spectra of 1 mM Esc(1-21) alone (A) and in the presence of (B) 200 mM perdeuterated DPC or (C) 125 mM perdeuterated SDS. Right Panel: Amide proton region of ^{1}H NMR spectra of 1 mM Esc(1-21)-1c alone (A) and in presence of (B) 200 mM perdeuterated DPC or (C) 125 mM perdeuterated SDS. The NMR experiments were performed using a Bruker Avance III 700 MHz spectrometer in aqueous solutions (pH ~4.5) at 37 ^{0}C.

Fig. 6. Summary of NOE contacts of Esc(1-21) and Esc(1-21)-1c peptides in the DPC micelles. Left panel: Bar diagram demonstrating different (sequential, medium range, and long range) NOE contacts in the NOESY spectra of Esc(1–21) (A) and Esc(1–21)-lc (B) in deuterated DPC micelles. The intensity of the NOESY peaks are designated by the thickness of the bars which are assigned as strong, medium, and weak during structure calculation. CαH/NH (i to i+3) NOEs are marked by blue bars and CαH/NH (i to i+4) NOEs are marked by red bars. Right panel: A histogram displaying the number and type (intra, sequential, medium) of NOEs of Esc(1-21) (C) and Esc(1-21)-lc (D) as a function of residue number in complex with DPC micelles. The NOESY experiments (mixing time 150 ms) were performed using Bruker Avance III 700 MHz spectrometer with 1 mM concentrations of peptides in aqueous solution (pH ~4.5) at 37 ^{0}C.

Fig. 7. Three dimensional solution structures of Esc(1-21) in DPC micelles (PDB ID 5XDJ). Superposition of backbone atoms (N, Cα, C′) of the 20 lowest energy conformations of Esc(1–21)

(A). Cartoon representation of side chain orientation of a representative NMR structure of Esc(1–21) showing different residues (B). Electrostatic potential surface of Esc(1–21) showing the distribution of polar and non-polar residues (C). The hydrophobic and positively charged amino acid residues are indicated by green and blue, respectively, while all other residues are in white.. These images were produced using the PyMOL and Chimera software.

Fig. 8. Three dimensional solution structures of Esc(1-21)-1c in DPC micelles. Superposition of backbone atoms (N, Cα, C′) of the 20 lowest energy conformations of Esc(1-21)-1c (A). Cartoon representation of side chain orientation of a representative NMR structure of Esc(1-21)-lc showing different residues (B). Electrostatic potential surface of Esc(1–21)-1c showing the distribution of polar and non-polar residues (C). The hydrophobic and positively charged amino acid residues are indicated by green and blue, respectively, while all other residues are in white. These images were produced using the PyMOL and Chimera software.

Fig. 9. Overlaid structures of Esc(1-21) (red) and Esc(1-21)-1c (green) in DPC micelles. The N-terminal helical segment (I2-N13) is superimposed nicely with a backbone RMS deviation of 0.482.

Fig. 10. ^{2}H solid state NMR spectra (A) and the corresponding S_{CD} order parameters profile (B) of POPE:POPE$^{2}H_{31}$:POPG (2:1:1) at T= 310K, in the absence (black line) and presence of 2 mole % Esc (1-21) (red line) and Esc (1-21)-lc (blue line), respectively, with an estimated uncertainty of ± 1%.

Figure 1

Click here to download high resolution image

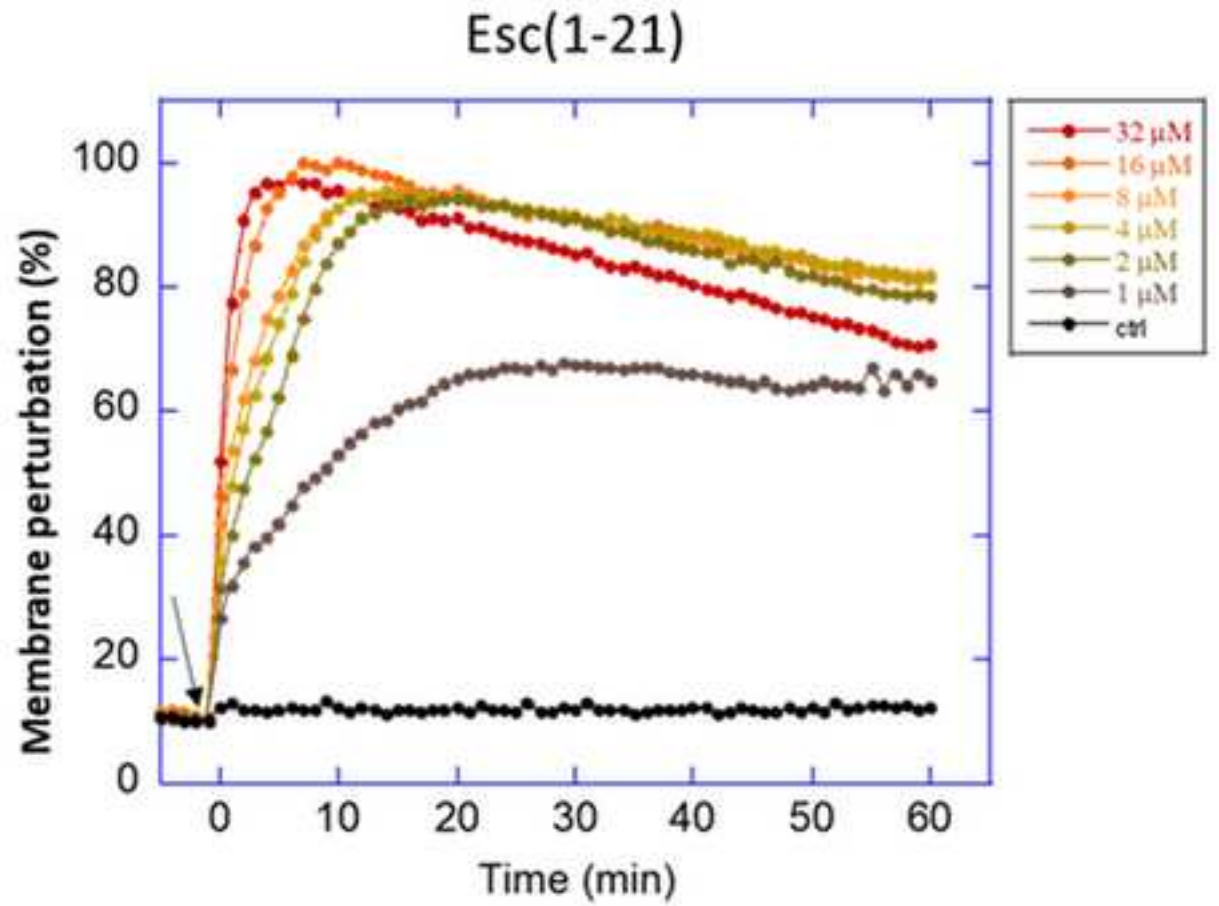

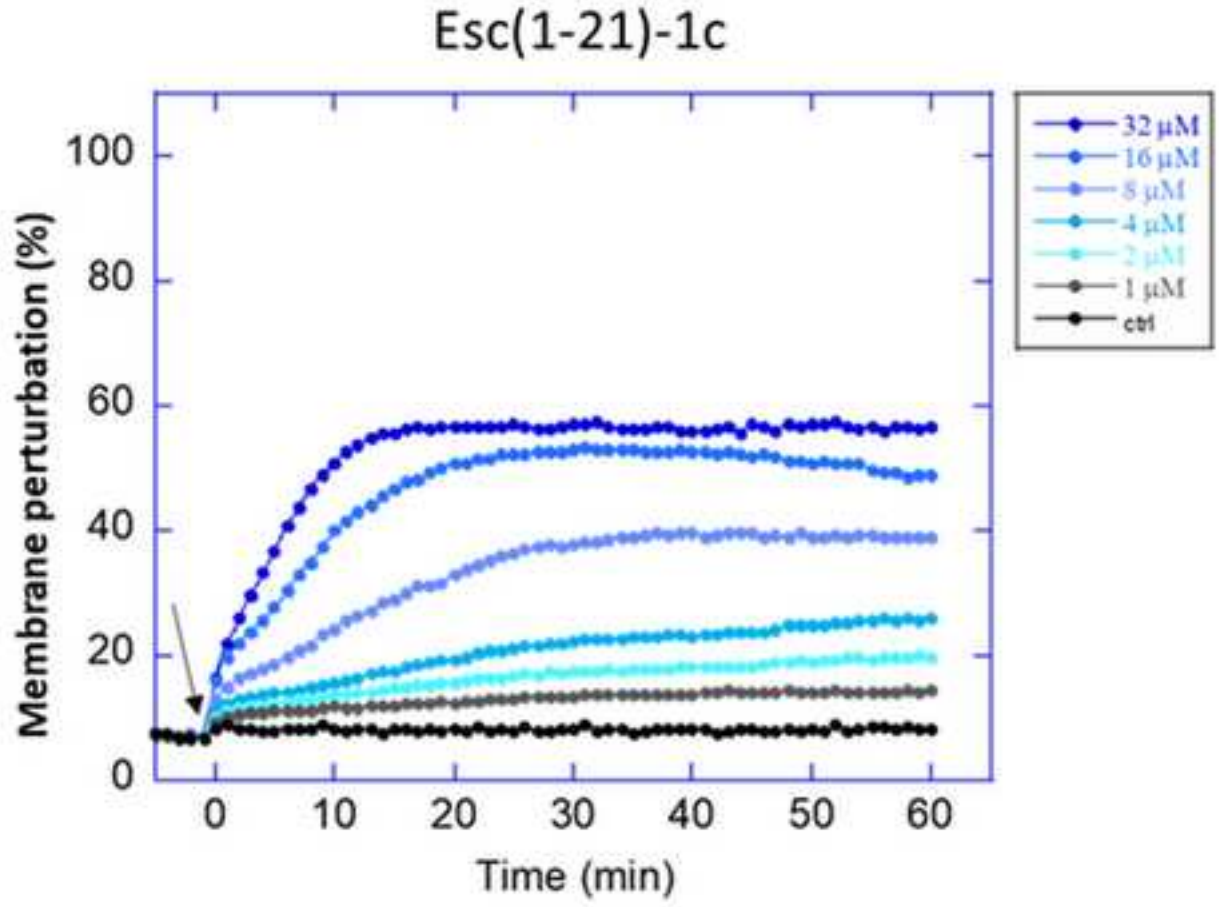

Figure 2

Click here to download high resolution image

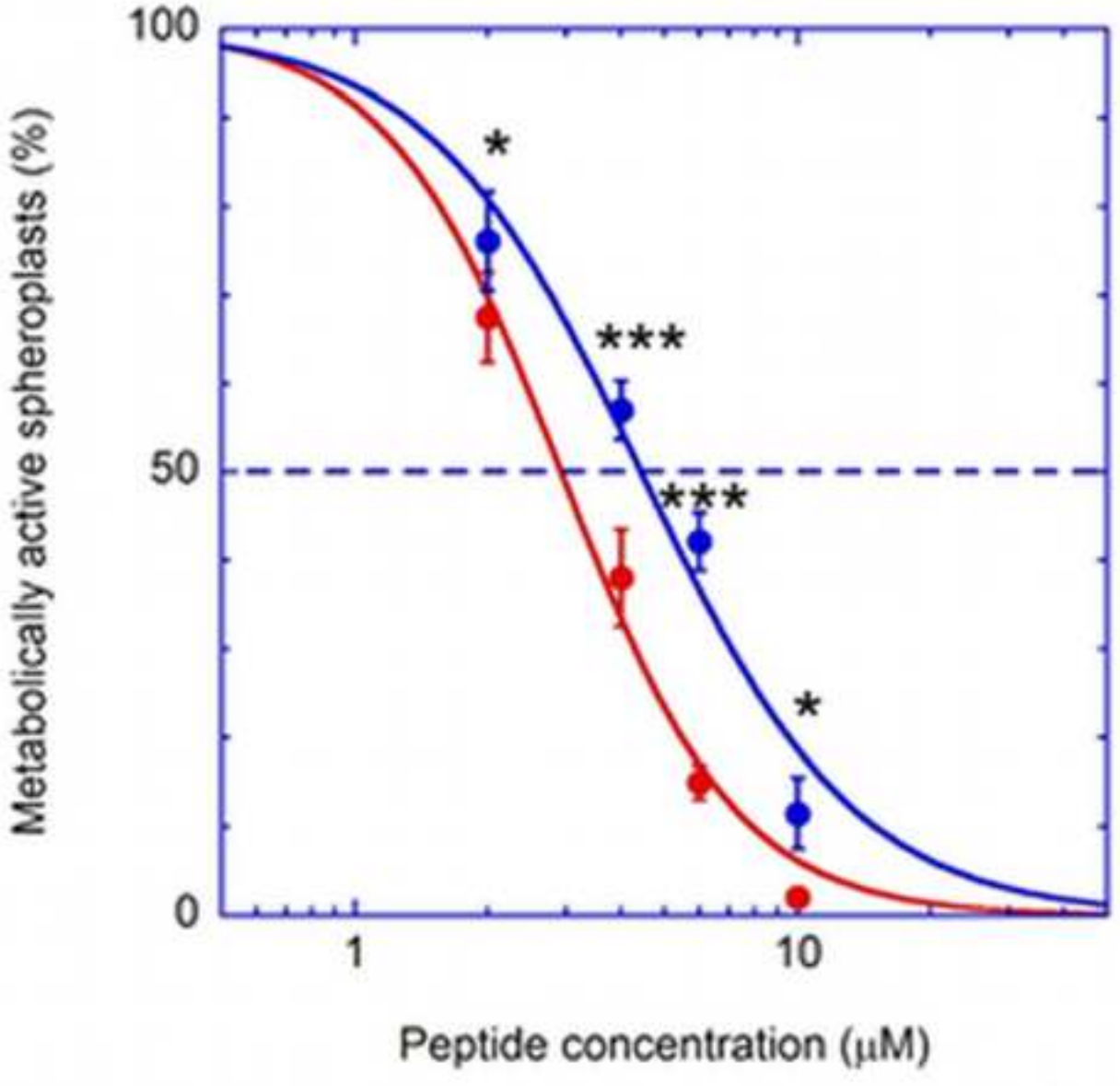

Figure 3

Click here to download high resolution image

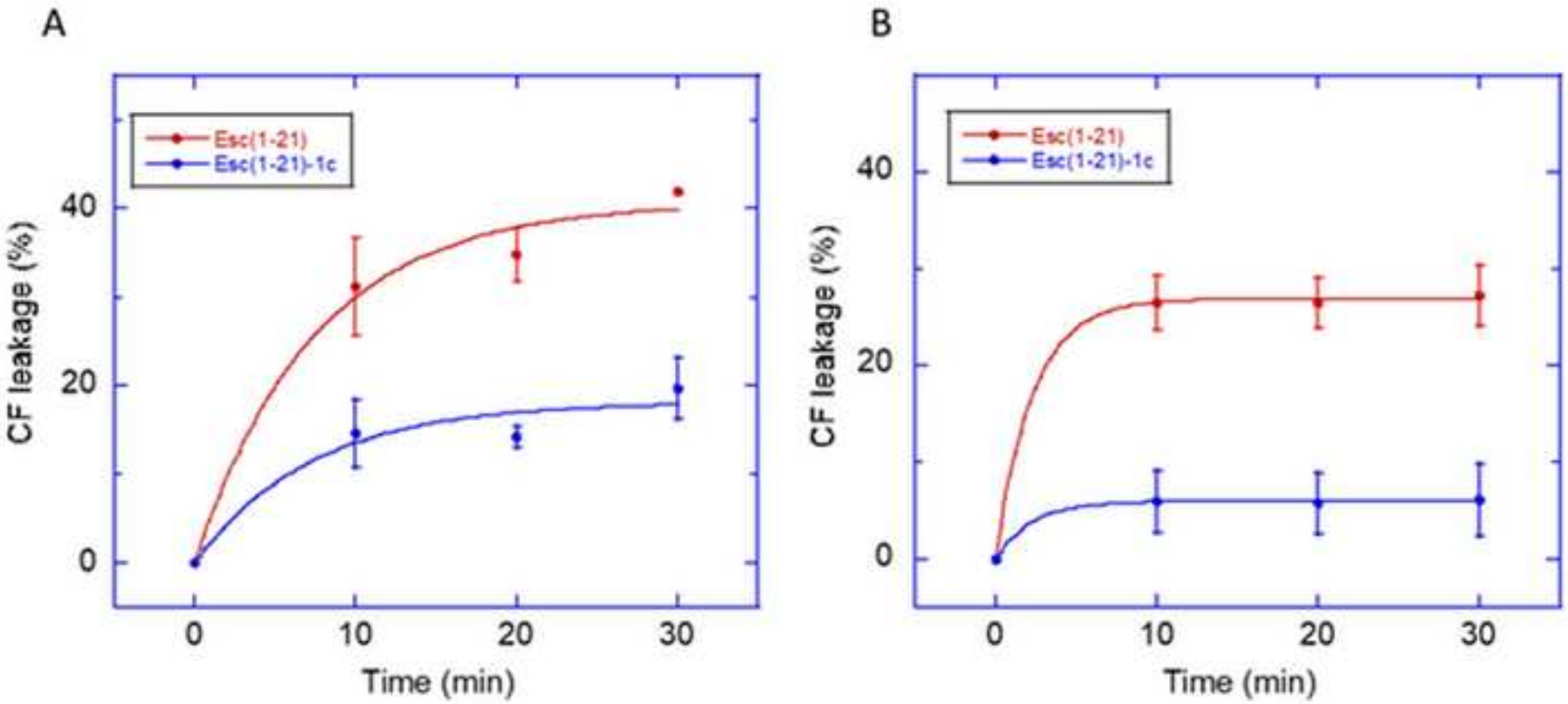

Figure 4

Click here to download high resolution image

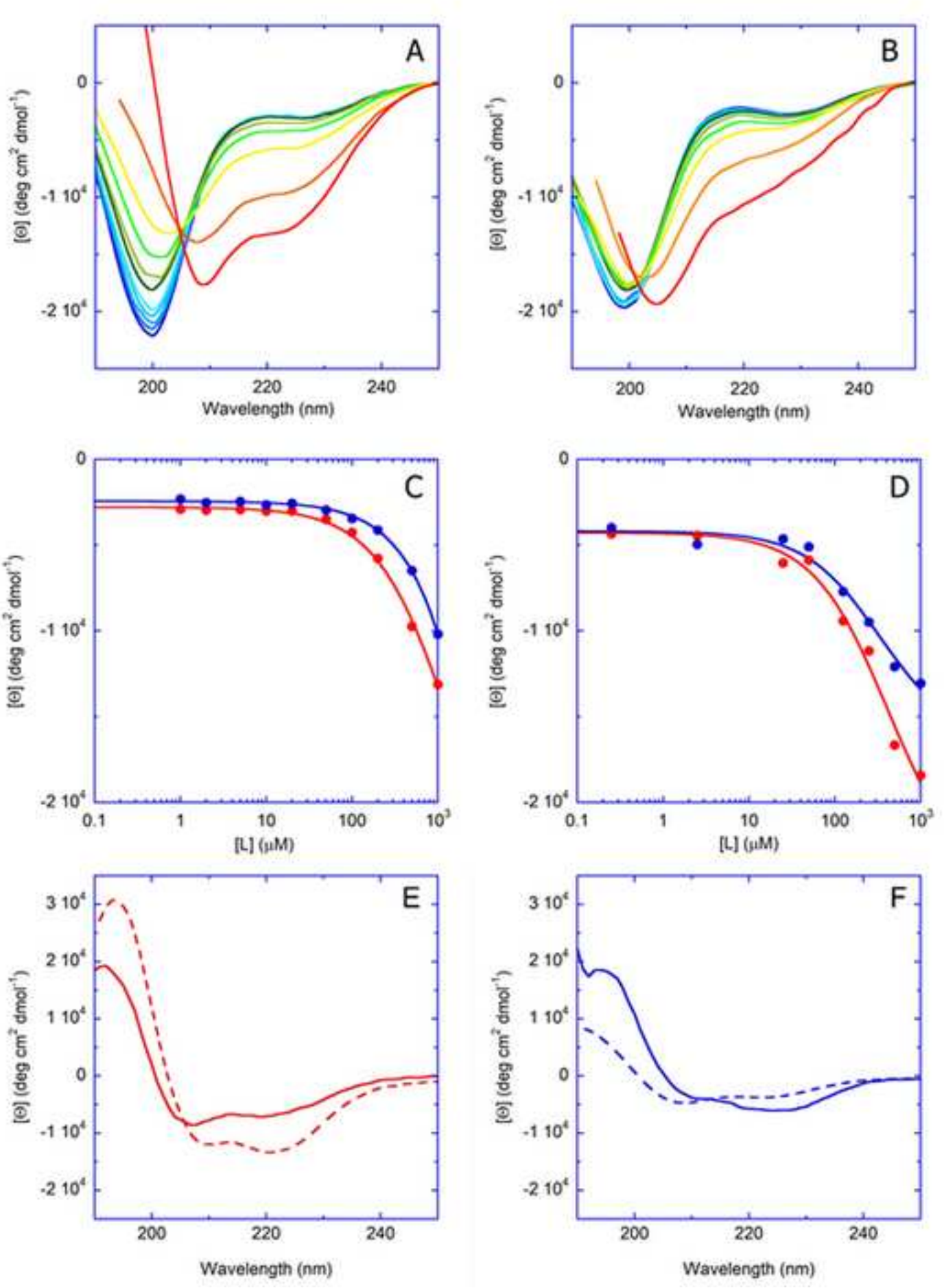

Figure 5

Click here to download high resolution image

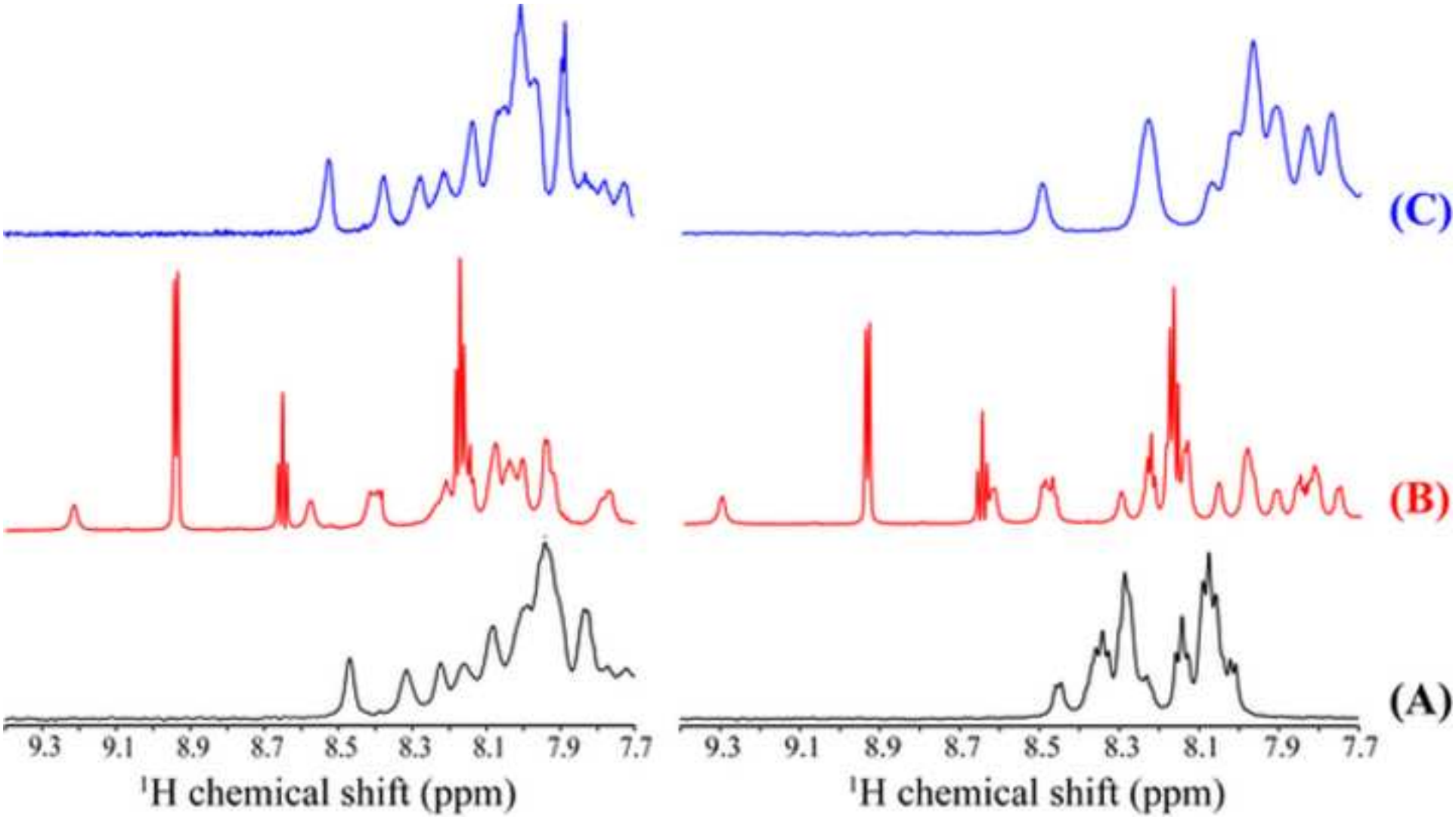

Figure 6

Click here to download high resolution image

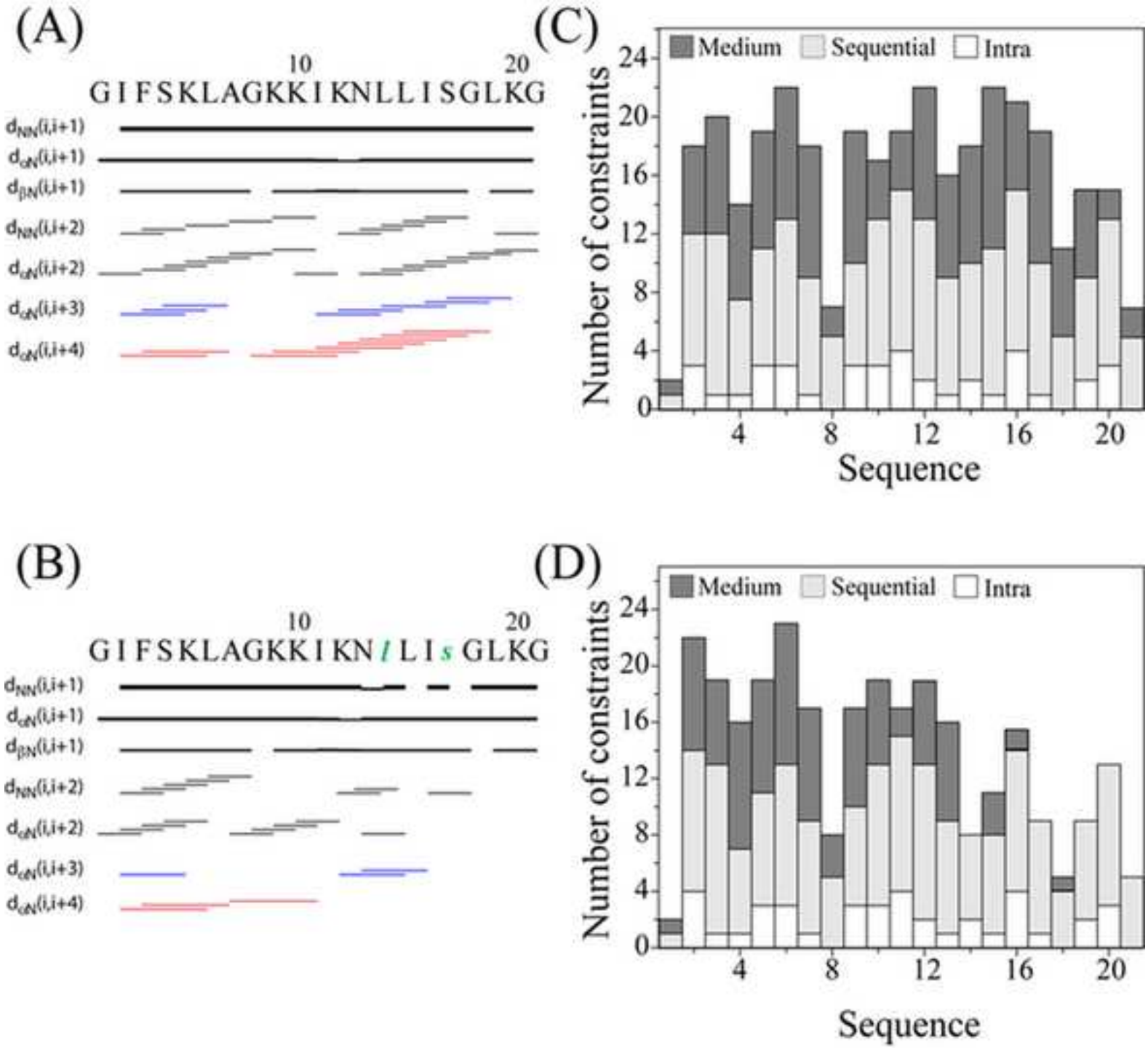

Figure 7

Click here to download high resolution image

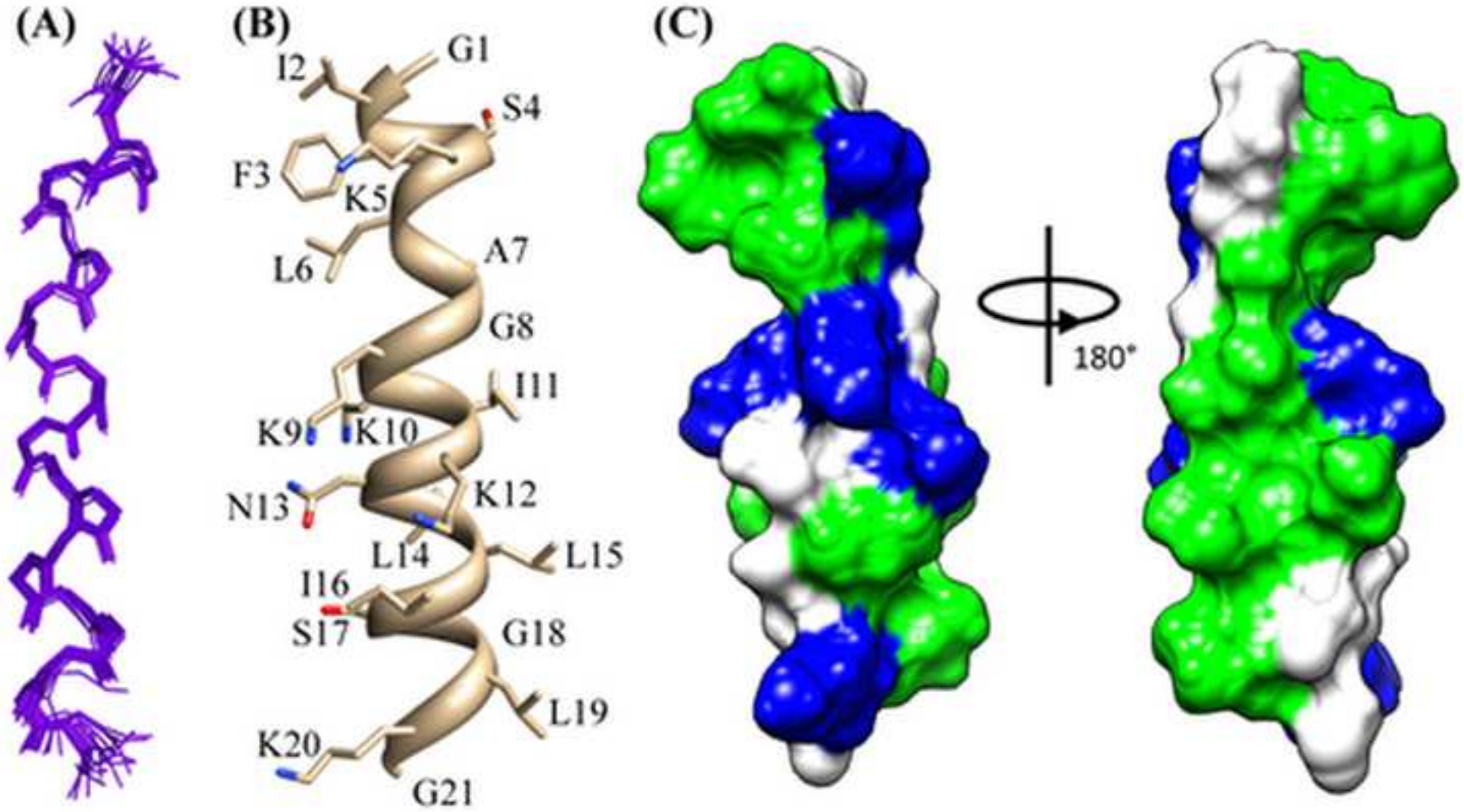

Figure 8

Click here to download high resolution image

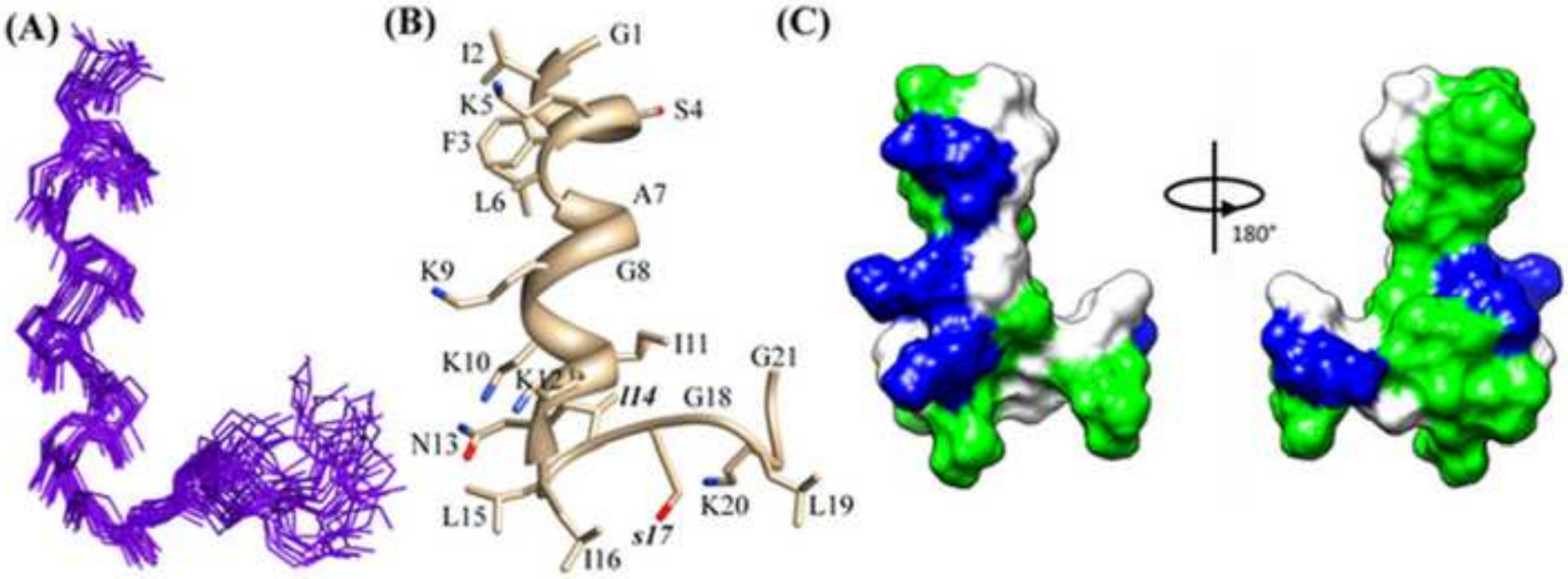

Figure 9

Click here to download high resolution image

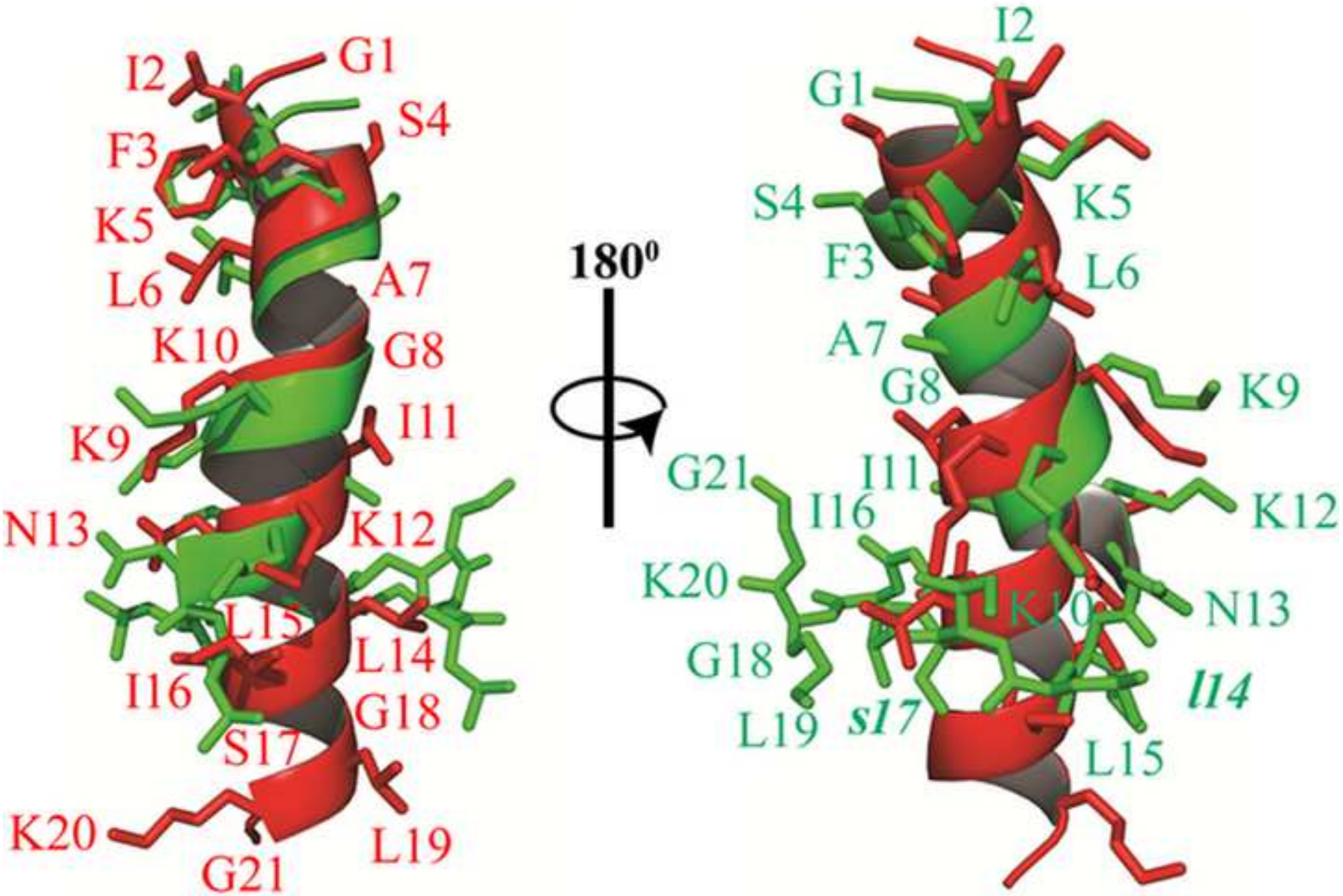

Figure 10

Click here to download high resolution image

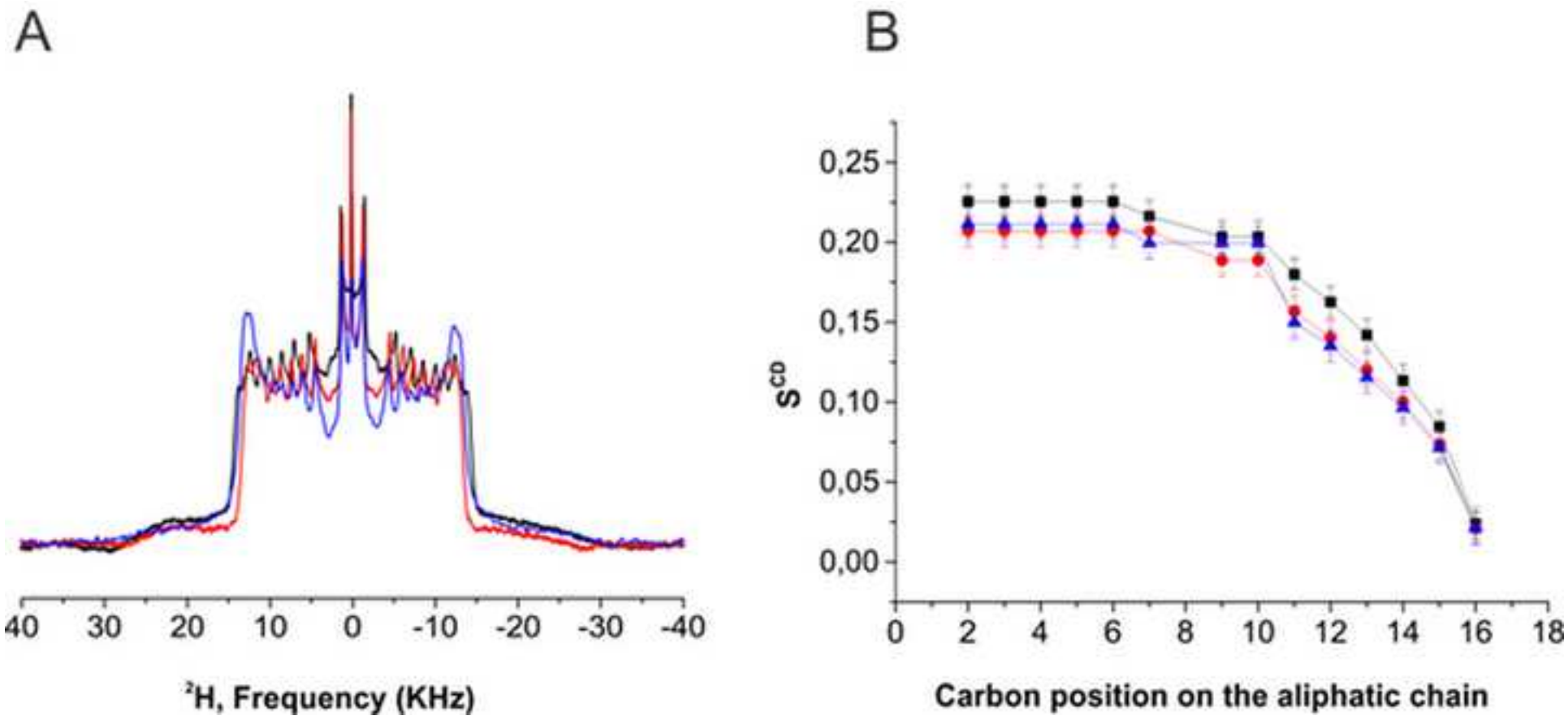

Supplementary Information

Membrane Perturbing Activities and Structural Properties of the Frog-skin Derived Peptide Esculentin-1a(1-21)NH_2 and its Diastereomer Esc(1-21)-1c: Correlation With Their Antipseudomonal and Cytotoxic Activity

Maria Rosa Loffredo[*,1] Anirban Ghosh[*,2] Nicole Harmouche,[3] Bruno Casciaro[1], Vincenzo Luca[1], Annalisa Bortolotti[4], Floriana Cappiello[1], Lorenzo Stella[4], Anirban Bhunia[2], Burkhard Bechinger,[3] and Maria Luisa Mangoni[1#]

*The authors equally contributed to the work

[1] Laboratory affiliated to Pasteur Italia-Fondazione Cenci Bolognetti, Department of Biochemical Sciences, Sapienza University of Rome, Rome, 00185, Italy; [2]Department of Biophysics, Bose Institute, P-1/12, CIT Road, Scheme VII (M), Kolkata 700054, India; [3]University of Strasbourg/CNRS, Chemistry Institute UMR 7177, 4 rue Blaise Pascal, 67070 Strasbourg, France; [4]University of Rome Tor Vergata, Department of Chemical Sciences and Technologies, 00133 Rome, Italy

To whom correspondence should be addressed

Maria Luisa Mangoni, PhD
Department of Biochemical Sciences,
Sapienza University of Rome.
Via degli Apuli, 9-00185, Rome-Italy;
Phone: +39 06 49917693
Fax: +39 0649917566
Email: marialuisa.mangoni@uniroma1.it

Supporting information Figures

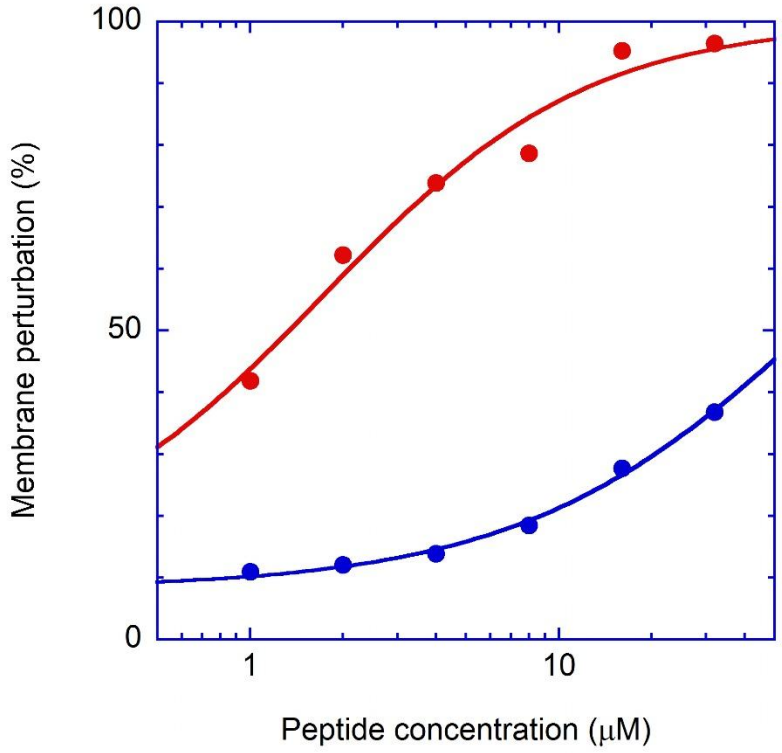

Figure S1. Dose-response of the cytoplasmic membrane permeabilization of the planktonic form of *P. aeruginosa* AA43 induced by different concentrations of Esc(1-21), red line, and Esc(1-21)-1c, blu line, 5 min after their addition to the bacterial cells. See legend to Fig. 1 for additional experimental details. Data points represent the mean of triplicate samples from a single experiment, representative of three different experiments.

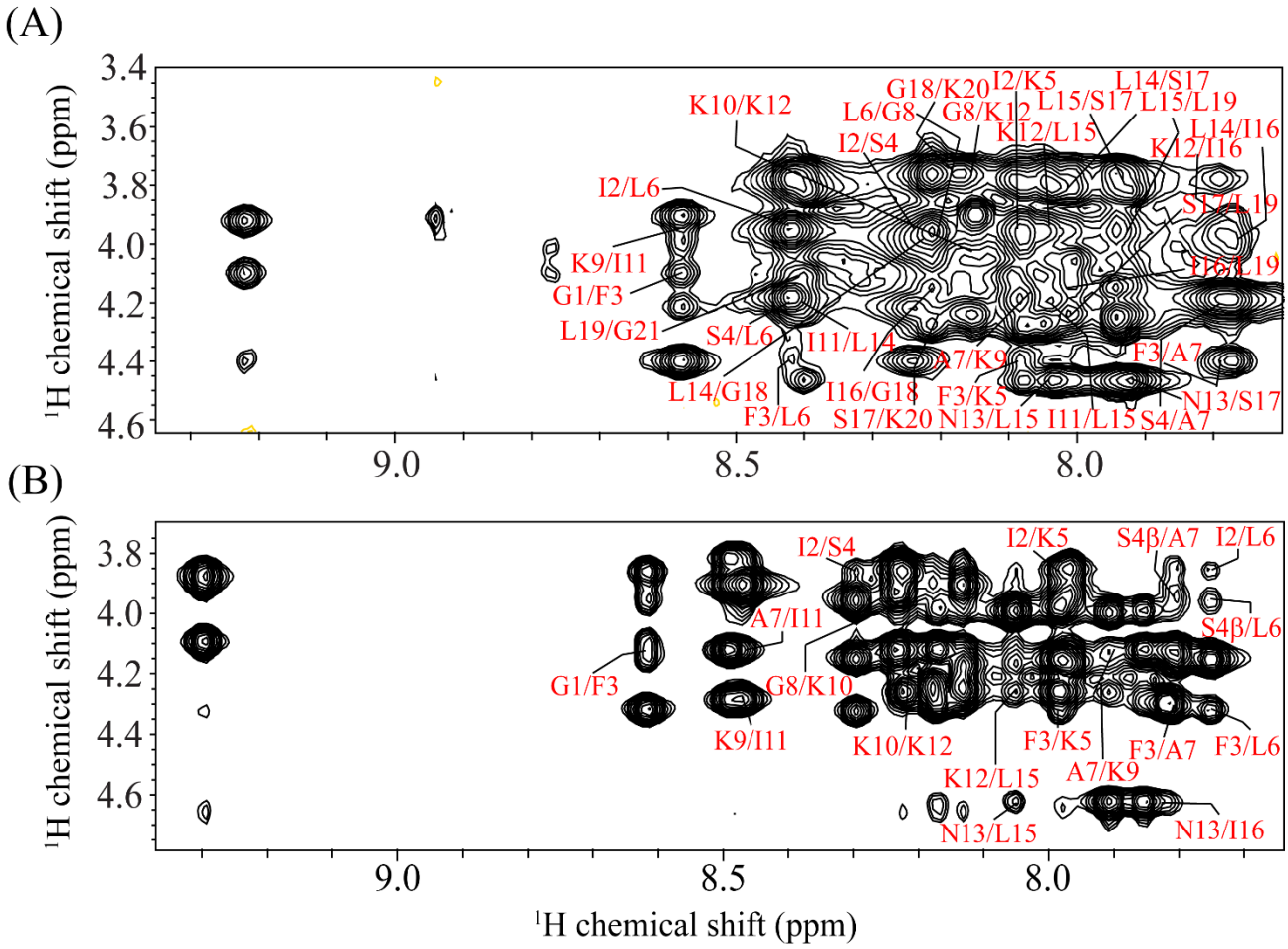

Figure S2. Finger print region of NOESY spectra of (A) Esc(1-21) and (B) Esc(1-21)-lc peptides in 200 mM perdeuterated DPC micelles. For clarity, only medium range NOE contacts were marked by red color. The NOESY experiments (mixing time 150 ms) were performed in Bruker Avance III 700 MHz spectrometer with 1 mM concentrations of peptides in aqueous solution (pH ~4.5) at 37 ^{0}C.

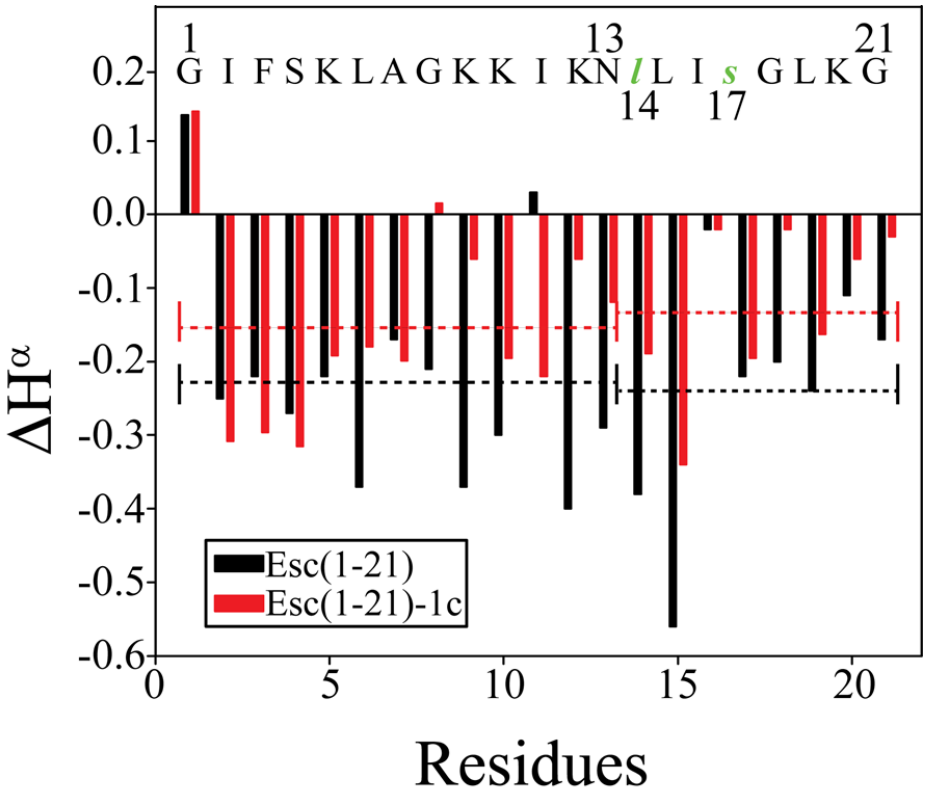

Figure S3. Chemical shifts deviations of the CαH resonances for each residues of either Esc(1-21) (black bar) or Esc(1–21)-1c (red bar) relative to standard chemical shift values. The peptide sequence is shown in the positive axis of the plot where D-amino acids are denoted by 'blue italics' notion. The average chemical shift deviations for (G1-N13) and (L14-G21) segment is shown by black and red dotted lines for both peptides respectively.

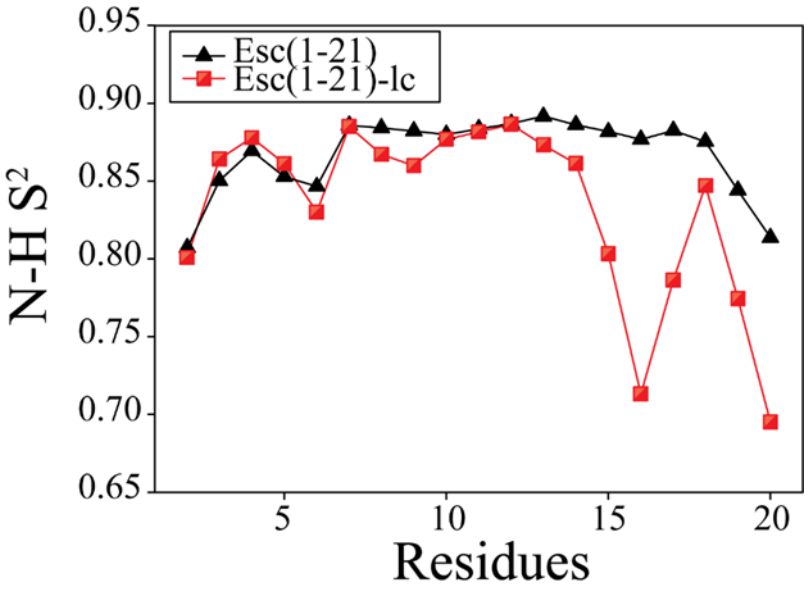

Figure S4. Residue specific N-H order parameter (S^2) calculated from the ensemble of 20 lowest energy structures of Esc(1-21) (black line) and Esc(1-21)-1c (red line) in DPC.

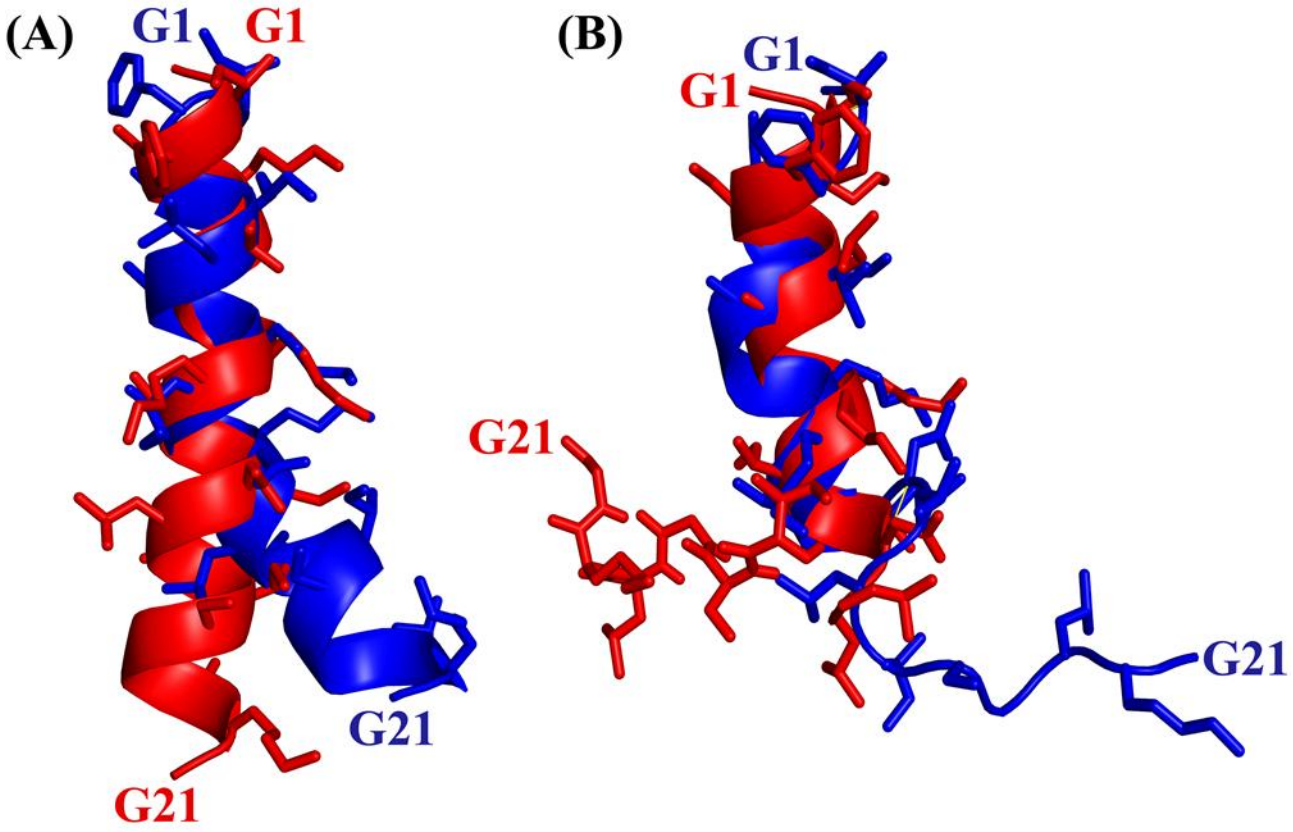

Figure S5. Overlaid structures of NMR derived conformation of (A) Esc(1–21) in LPS (blue) and) Esc(1–21) in DPC (red) micelles (B) Esc(1–21)-lc in LPS (blue) and Esc(1–21)-lc in DPC micelles (red). The N-terminal helical segment (Ile2-Asn13) is superimposed with a backbone RMSD of 1.921 (A) and 1.70 (B) respectively. The coordinates for NMR derived conformations of two peptides in LPS were taken from our earlier study [42].

***Conflict of Interest**

Click here to download Conflict of Interest: coi_disclosure.pdf